Remote Sensing of Environment 270 (2022) 112856

Contents lists available at ScienceDirect

Remote Sensing of Environment

journal homepage: www.elsevier.com/locate/rse

Combining near-infrared radiance of vegetation and fluorescence spectroscopy to detect effects of abiotic changes and stresses

Yelu Zeng [a,b], Min Chen [a,*], Dalei Hao [c,*], Alexander Damm [d,e], Grayson Badgley [b,f], Uwe Rascher [g], Jennifer E. Johnson [b], Benjamin Dechant [h], Bastian Siegmann [g], Youngryel Ryu [h,m], Han Qiu [a], Vera Krieger [g], Cinzia Panigada [i], Marco Celesti [j], Franco Miglietta [k], Xi Yang [l], Joseph A. Berry [b]

[a] Department of Forest and Wildlife Ecology, University of Wisconsin-Madison, 1630 Linden Drive, Madison, WI, USA
[b] Department of Global Ecology, Carnegie Institution for Science, Stanford, CA 94305, USA
[c] Atmospheric Sciences and Global Change Division, Pacific Northwest National Laboratory, Richland, WA, USA
[d] Department of Geography, University of Zurich, Winterthurerstrasse 190, 8057 Zurich, Switzerland
[e] Eawag, Swiss Federal Institute of Aquatic Science and Technology, Überlandstrasse 133, 8600 Dübendorf, Switzerland
[f] Black Rock Forest, Cornwall, NY 12518, USA
[g] Institute of Bio- and Geosciences, IBG-2: Plant Sciences, Forschungszentrum Jülich GmbH, Leo-Brandt-Str., Jülich 52425, Germany
[h] Research Institute of Agriculture and Life Sciences, Seoul National University, Seoul, South Korea
[i] Remote Sensing of Environmental Dynamics Laboratory, Department of Environmental and Earth Sciences, University of Milano - Bicocca, Milano, Italy
[j] HE Space for ESA - European Space Agency, ESTEC, Keplerlaan 1, PO Box 299, NL-2200, AG, Noordwijk, the Netherlands
[k] Institute for Bioeconomy (IBE), National Research Council (CNR), Via Caproni, 8 - 50145 Firenze, Italy
[l] Department of Environmental Sciences, University of Virginia, Charlottesville, VA, USA
[m] Department of Landscape Architecture and Rural Systems Engineering, College of Agriculture and Life Sciences, Seoul National University, South Korea

ARTICLE INFO

Editor: Marie Weiss

Keywords:
Solar-induced chlorophyll fluorescence (SIF)
Near-infrared radiance of vegetation
Fluorescence yield (Φ_F)
Low-light adaptation
Heat stress
Water limitation

ABSTRACT

Solar-induced chlorophyll fluorescence (SIF) shows great potential to assess plants physiological state and response to environmental changes. Recently the near-infrared reflectance of vegetation (NIRv) provides a promising way to quantify the confounding effect of canopy structure in SIF, while the difference between SIF and NIRv under varying environmental conditions has not been well explored. Here we developed a simple approach to extract the fluorescence yield (Φ_F) by the combined use of SIF and the near-infrared radiance of vegetation (NIRvR). The proposed NIRvR approach was evaluated in multiple ways, including with the seasonal leaf-level steady-state fluorescence yield. Results indicate that NIRvR-derived Φ_F well captured the seasonal variation of the fluorescence yield changes, and achieved similar results with the existing approach. Both SIF and NIRvR were derived from the airborne imaging fluorescence spectrometer HyPlant for three case studies to evaluate the impacts of light adaptation, heat stress and water limitation on Φ_F. For the light adaptation case study, Φ_F over the low-light adapted sugar beet field was about 1.3 times larger compared to an unaffected reference area while the difference in NIRvR was minimal, which clearly shows the short-term photosynthetic light induction effect and the ability of SIF to detect plant physiological responses. For the heat stress experiment, Φ_F decreased during a natural heatwave in 2015 in the fields of rapeseed from 0.0150 to 0.0130, barley from 0.0152 to 0.0144, and wheat from 0.0146 to 0.0142 which showed signs of senescence, while slightly increased from 0.0125 to 0.0130 in the corn field which was still in growing. At the water-limited sugar beet field, Φ_F first increased towards solar noon and then slightly decreased during the afternoon over the water-limited areas from 0.017 to 0.021 and 0.020, with high temperature and high light at noon. The advantages to use SIF/NIRvR as a proxy of Φ_F to detect stress-induced limitations in photosynthesis include that the impacts of canopy structure and sun-sensor geometry on the Φ_F estimation are explicitly cancelled, and photosynthetically active radiation (PAR) is not required as input. Finally, our approach is directly applicable to satellite-derived estimates of SIF, enabling the study of variations in Φ_F to detect the effects of abiotic changes and stresses at large scale.

* Corresponding authors.
E-mail addresses: mchen392@wisc.edu (M. Chen), dalei.hao@pnnl.gov (D. Hao).

https://doi.org/10.1016/j.rse.2021.112856
Received 25 February 2021; Received in revised form 10 December 2021; Accepted 16 December 2021
Available online 7 January 2022

1. Introduction

Solar-induced chlorophyll fluorescence (SIF) has been regarded as a breakthrough to monitor vegetation photosynthesis, detect environmental stress effects in plants, and estimate crop yield (Frankenberg et al., 2011; Guan et al., 2016; Guanter et al., 2014; Magney et al., 2019). Compared to many optical remote sensing vegetation indices, SIF is less impacted by soil background, conveys leaf physiology information and is considered as a direct measure of energy available for carbon-fixation for estimating photosynthesis (Magney et al., 2020; Mohammed et al., 2019; Sun et al., 2017; Yang et al., 2015). Ample evidence suggests that apparent canopy SIF retrieved from remote sensing data is substantially affected by sun-sensor geometry and canopy structure (Hao et al., 2021; He et al., 2017; Porcar-Castell et al., 2014; Zhang et al., 2018). Only a proportion of the total emitted SIF photons by all plant leaves can escape from the canopy, which hinders the direct linkage between apparent canopy SIF and emitted SIF from leaf. This variable proportion between SIF at the leaf and canopy scales can be quantified by the directional or hemispherical photon escape ratio (f_{esc}) of a canopy at a certain sun-sensor geometry (Zeng et al., 2019), and this effect needs to be accounted for prior to using SIF to estimate gross primary productivity (GPP) (Dechant et al., 2020; Liu et al., 2020; Zhang et al., 2020) and fluorescence yield (Φ_F) (Wang et al., 2020).

Several radiative transfer models and machine learning-based approaches were developed to quantify f_{esc} and thus convert apparent canopy SIF to total emitted SIF by all leaves (Liu et al., 2019; Romero et al., 2018; Zeng et al., 2020). Because far-red SIF and near-infrared (NIR) photons of vegetation (NIRv for reflectance) share the same f_{esc} and anisotropic distributions, Zeng et al. (2019) proposed a simple approach based on the spectral invariants theory to estimate f_{esc} (i.e. as ratio between NIRv and the fraction of absorbed photosynthetically active radiation (FPAR)) to correct the sun-sensor geometry effect on SIF. A byproduct of this development was the finding that SIF and NIRv are physically related (Zeng et al., 2019), a fact that complements the already observed similar performances of SIF and NIRv when estimating GPP (Badgley et al., 2017; Li et al., 2018). The similarity between SIF and NIRv has been explored in several subsequent studies (Dechant et al., 2020; Turner et al., 2020; Wu et al., 2020), while their differences have not been systematically quantified under environmental changes and stresses (He et al., 2020).

There are still obvious differences between SIF and NIRv, particularly occurring under highly variable illumination and environmental stresses. There is in fact a conceptual difference between SIF, which is strongly driven by photosynthetically active radiation (PAR), and surface reflectance-based vegetation indices (e.g., NIRv) that are theoretically independent of PAR. Deriving f_{esc} from a NIRv-based approach applicable for SIF must ensure that both SIF and NIRv include the similar dependency on the ratio of diffuse radiation and sun-sensor geometry. To be comparable with SIF regarding the solar radiation dependence and unit, Zeng et al. (2019) derived the radiance version of NIRv by the product of NDVI times the upwelling NIR radiance (NDVI×NIRrad), which was firstly called NIRv' in Zeng et al. (2019) and later was called near-infrared radiance of vegetation (NIRvR) in Dechant et al. (2020). NIRvR was recently found to have a strong relationship with GPP over both sparse and dense canopies (Baldocchi et al., 2020; Wu et al., 2020; Liu et al., 2020).

SIF dynamics at the canopy scale can be described as the product of three contributors: absorbed PAR (APAR: μmol m^{-2} s^{-1} or W m^{-2}), physiological response (fluorescence yield, Φ_F: unitless for the whole SIF spectrum and nm^{-1} for a given wavelength), and canopy structure (f_{esc}: sr^{-1}) (Guanter et al., 2014). Early studies on the response of observed SIF to stress showed promising results but did not account for the impacts of f_{esc} driven by the canopy structure effect and sun-sensor geometry (Wieneke et al., 2016; Wieneke et al., 2018; Wohlfahrt et al., 2018; Wen et al., 2020). Not accounting for f_{esc} can lead to challenges in interpreting responses of SIF to stresses (Wang et al., 2020; He et al., 2020), as the structural response by f_{esc} cannot be separated from the physiological response by Φ_F, which is unique to SIF and was found to be sensitive to environmental stress (Flexas et al., 2002; Porcar-Castell et al., 2014; Helm et al., 2020). The co-variations of f_{esc} with spatial, temporal and viewing geometry across biomes can lead to systematic biases in understanding SIF dynamics if Φ_F was not isolated from the impacts of f_{esc} (Wang et al., 2020).

Recent studies used SIF/(PAR × FPAR) to normalize the irradiance dependency of SIF and calculate Φ_F, while ignore the large uncertainties in the required FPAR and PAR at both the field and satellite levels (Gamon et al., 1995; Guanter et al., 2014; Yang et al., 2015). More recently, a few studies began to use PAR and vegetation indices, e.g., NIRv together with SIF to approximate Φ_F and detect effects of abiotic changes and stresses as SIF/(PAR × NIRv) (Dechant et al., 2020; Wang et al., 2020), namely the 'NIRvP' approach. Sometimes NIRv can be replaced with the Fluorescence Correction Vegetation Index (FCVI) and Φ_F is approximated by SIF/(PAR × FCVI) (Yang et al., 2020; Siegmann et al., 2021). This 'NIRvP' approach avoids introducing FPAR but still require PAR, and may introduce uncertainties if sensors with opportunities for SIF. For example, the TROPOspheric Monitoring Instrument (TROPOMI) onboard the Sentinel-5 Precursor satellite mission, does not have a corresponding simultaneous PAR (i.e. 400 nm ~ 700 nm) product and only samples a smaller spectral window (e.g., 675 nm ~ 775 nm for TROPOMI) (Guanter et al., 2015). Using a PAR product from other sources may lead to spatio-temporal mismatches and discrepancies between SIF observations and the concurrent PAR needed, due to different overpass times or the corresponding daily upscaling. Compared to satellite observations with coarse spatio-temporal resolution, it is important to understand the impact of f_{esc} and PAR on the sensitivity of SIF for plant response to environmental stress using high-resolution spectroscopy airborne data, e.g., the imaging spectrometer HyPlant (Rascher et al., 2015; Siegmann et al., 2019).

The objective of this study is to develop an alternative approach to estimate the Φ_F variations especially when simultaneous PAR is unavailable, to evaluate the validity of the proposed method, and to evaluate the Φ_F changes in response to light adaptation, heat stress and water limitation conditions using the datasets from the airborne HyPlant imagery. We anticipate that NIRvR provides a potential pathway to normalize SIF for both the canopy structure effects and solar illumination conditions (with the unit of radiance instead of reflectance), and thereby to reliably extract the variations of canopy-scale Φ_F to detect effects of abiotic changes and stresses on vegetation canopies. We therefore aim to i) characterize spatial and temporal differences in SIF and NIRvR under abiotic changes and stresses, and ii) evaluate whether the canopy-scale Φ_F derived from normalization of SIF by NIRvR can capture the physiological response to environmental drivers.

Below we first introduced the theoretical basis of our 'NIRvR' approach to estimate canopy-scale Φ_F by combining SIF and NIRvR, and evaluated the performance of the proposed approach with field data, modeling experiments and the results by using the NIRvP approach. We then compared the responses of SIF, NIRvR and Φ_F to extreme environmental conditions using airborne high-resolution spectroscopy data acquired with the imaging spectrometer HyPlant. In particular, our analyses include observations from a light adaptation case study including short-term photosynthetic light induction (the shadowing effect and the light exposure), as well as heat stress and water limitation in crop fields. Finally, we discuss the complementary benefits of the new approach for a more robust usage of SIF in vegetation stress assessments.

2. Theoretical derivations

According to Zeng et al. (2019) and Dechant et al. (2020), the linkage between sensor-observed far-red SIF and NIRvR of a canopy at a given sun-sensor geometry can be expressed as:

$$SIF_N = PAR \cdot FPAR_{chl} \cdot \Phi_F \cdot f_{esc} \quad (1a)$$

$$NIRvR = INIR \cdot i_{0,green} \cdot w_N \cdot f_{esc} \quad (1b)$$

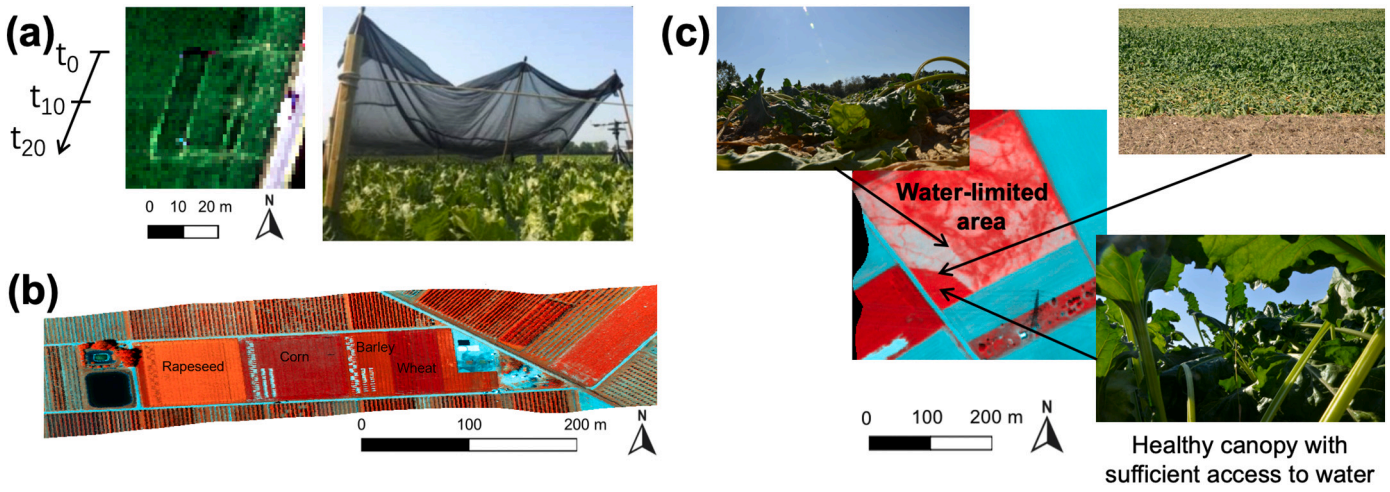

Fig. 1. The three case studies of light adaptation (a), heat stress (b) and water limitation (c). (a) shows the light adaptation study site (the virtual cloud experiment) in true color HyPlant image (left) and in situ photograph (right). t_i in (a) represents the time (unit: minute) for the pixel that the shading net was removed already before the HyPlant overflight. (b) shows the heat stress study site as false color Hyplant image. Further details can be found in (Yang et al., 2019). (c) shows the water limitation study site in false color HyPlant image, which is surrounded by photographs that show a canopy in water limitation (top-left), a healthy canopy (bottom-right) and both canopies combined (top-right). Most parts of the field in (c) were in water limitation compared to a small reference corner with sufficient access to water.

where SIF_N is the far-red SIF at 760 nm (unit: mW m^{-2} sr^{-1} nm^{-1}), $FPAR_{chl}$ is the fraction of absorbed PAR by chlorophyll, Φ_F is the fluorescence yield in the NIR band (unit: nm^{-1} for a given wavelength), INIR is the incoming NIR irradiance at the bottom of atmosphere for a certain NIR wavelength (unit: mW m^{-2} nm^{-1}), f_{esc} is the photon escape ratio for far-red SIF and NIR photons (unit: sr^{-1} for directional observations), $i_{0,green}$ is the canopy directional interceptance (unitless) of green components with chlorophyll, and w_N is the green leaf single scattering albedo in the NIR band (unitless). Note $i_{0,green}$ is not the total interceptance by all the plant components (total i_0), considering the possible non-green leaves contribution during abiotic changes. The non-green components will not contribute to $i_{0,green}$ and NIRvR by definition (NIR radiance of green vegetation, with more strict definition here). In practice, NIRvR is calculated as NDVI×NIRrad, and thus non-green components (e.g., dry matter with almost flat spectrum in red-NIR wavelength) have non-zero NIR reflectance and radiance but have near-zero NDVI and NIRvR. Therefore, both NIRvR and SIF are minimally impacted by non-green components. In fact, the role of non-green leaves on NIRvR is the same as other backgrounds, e.g., the soil and trunk. The green i_0 and green FPAR have a strong linear relationship with a coefficient of determination (R^2) of 0.99 and a root-mean-square-error (RMSE) of 0.03 in the simulation with a wide variety of vegetation variables (Zeng et al., 2019).

f_{esc} can be cancelled out by dividing Eq.(1a) by Eq.(1b) and we can get

$$\Phi_F = SIF_N/NIRvR\cdot(INIR/PAR)\cdot\left(i_{0,green}/FPAR_{chl}\right)\cdot w_N \quad (2)$$

Note that INIR is a stably correlated to the incoming PAR at a given ratio of diffuse radiation (Dechant et al., 2020; Liu et al., 2020), $FPAR_{chl}$ is a good approximation of the directional interceptance $i_{0,green}$ by chlorophyll *a*t various canopy structure/sun-sensor geometry on sunny days (Zeng et al., 2019), and the NIR leaf albedo (w_N) does not change with leaf chlorophyll content (Ollinger, 2011) and can be regarded as a constant term in this study. Therefore, Φ_F is proportional to $SIF_N/NIRvR$, suggesting that $SIF_N/NIRvR$ can represent the variability of Φ_F:

$$\Phi_F \propto SIF_N/NIRvR \quad (3)$$

To acquire NIRvR, Zeng et al. (2019) showed that

$$NDVI\cdot NIR \approx NIRv = i_{0,green}\cdot w_N\cdot f_{esc} \quad (4)$$

where NIR is the reflectance in the NIR band. Combining Eq. (1b) and Eq. (4), we can get

$$NIRvR = INIR\cdot NIRv \approx INIR\cdot NDVI\cdot NIR = NDVI\cdot NIRrad \quad (5)$$

where NIRrad is the upwelling NIR radiance. Eqs. (2)–(5) suggest the variability of Φ_F can be simply represented by $SIF_N/NIRvR$, and NIRvR can be estimated by the product of NDVI times the upwelling NIR radiance. Note that $SIF_N/NIRvR$ does not indicate the absolute value of Φ_F, instead acts as a linear approximation of Φ_F (we refer it to the relative Φ_F) to indicate its variability in response to environmental conditions and stresses. Hereafter we use SIF instead of SIF_N for short as this study will only discusses the far-red SIF, and keep using Φ_F to represent $SIF_N/NIRvR$ for the simplicity purpose.

3. Methods and dataset

3.1. Evaluating the NIRvR approach

We first evaluated the NIRvR approach in multiple ways. We started by comparing the Φ_F estimated by NIRvR against the continuous seasonal leaf-level steady-state fluorescence yield (Fs) measurements by the active pulse-amplitude modulated (PAM) fluorimetry during 2017–2018 at the evergreen needleleaf forest-dominated Niwot Ridge ecological research site (Magney et al., 2019), where the corresponding NDVI, PAR and NIR radiance measurements were also available. We acknowledge that there is potential scale mismatch between the leaf-level measurements and the NIRvR-derived Φ_F which represents the canopy-scale average, but this is the best available dataset for the benchmarking since the canopy-scale Φ_F is not directly measurable so far. The dataset was also suitable for our comparison because we only intended to evaluate the seasonal variation of Φ_F rather than the absolute values.

We then used the Soil Canopy Observation, Photochemistry and Energy (SCOPE) model (van der Tol et al., 2009) version 1.70 to evaluate the NIRvR-derived Φ_F by taking the model-simulated Φ_F as the 'true' values. NIRvR-derived Φ_F was calculated as the top-of-canopy SIF divided by NIRvR, and the 'true' values were calculated as the total emitted SIF by all leaves divided by APAR of the canopy. The SCOPE simulations were driven by a wide range of soil-leaf-canopy and environmental parameters to represent a variety of conditions. More details

about the model setup can be found in Table S1. In addition, we also examined the effects of noise occurring under observational conditions on the SIF and NIRvR measurements. HyPlant far-red SIF observations have been reported to have a rRMSE of 8.7% against the ground-based SIF measurements (Rascher et al., 2015), and thus we prudently set a white noise of 10% of the absolute value for SIF. The NIR surface reflectance measurements are usually more accurate than SIF measurements from the same sensor, and thus 5% white noise were used for NIRvR. The noises were added by Latin Hypercube Sampling. The correlation coefficients (R) between the true Φ_F and the NIRvR-derived Φ_F were calculated after repeating the noise sampling for 10, 000 times.

Finally, we compared the similarity between Φ_F derived from the NIRvR and the NIRvP approaches at an irrigated agricultural research site (41°9′53.64"N, 96°28′12.36"W) at the Eastern Nebraska Research and Extension Center of University of Nebraska-Lincoln. The site had repeated half-hourly top-of-canopy SIF, NIRv, NIR radiance, and PAR measurements available during the crop growing season in 2017 and 2018, thus, we calculated Φ_F using both the NIRvR and NIRvP approaches. The site had a corn-soybean rotation over the study period. More details can be found in Wu et al. (2020).

3.2. Case studies with the HyPlant experiments

Three case studies were conducted independently to assess the sensitivity of SIF, NIRvR and derived Φ_F for a dynamic adaptation of vegetation physiology caused by environmental factors including shade-light transition, as well as heat stress and water limitation. The light adaptation and heat stress case studies were conducted in two areas of the agricultural research station Campus Klein-Altendorf located near Bonn, Germany. The water limitation case study was conducted in the area of the Rur catchment close to the city of Jülich, Germany (Simmer et al., 2015).

The light adaptation case study was carried out over a sugar beet field (50°37′3.77"N, 6°59′19.20″E) on July 1st, 2015. The airborne imagery was acquired at 3:14 pm from 350 m above ground level, leading to a spatial resolution of 0.5 m × 1 m. The sugar beet plants were covered by a 6 m × 30 m shading net 0.5 m above the canopy for at least one hour (Fig. 1a). The 50% reduced solar irradiance yielded in a low-light adaptation of the sugar beet plants. The light adaptation case study mimicked the virtual cloud experiment with the effect of a shadow and quick light exposure. This dynamic observations after low light adaptation resemble the Kautsky effect, typically observed after dark adaptation, which is well known from lab and field experiments (Gomez-Chova et al., 2006; Flexas et al., 2012). The black cover was removed starting 20 min before the airborne sensor flew over from north to south. This allowed to expose plants to high light conditions for different periods before the airplane overpass and induce the shadowing effect. The last portion of the net was removed right before the aircraft's arrival, so the airborne sensor was capable of registering all the phases of the light adaptation transient (see also ESA report, 2015).

The heat stress case study site (50°37′24.93″N, 6°59′25.11″E) was closely located to the light adaptation case study at the Campus Klein-Altendorf. During a natural heatwave lasting from July 1st to 5th with maximum air temperature on each day exceeding 30 °C, several crops were measured before (i.e. at 3:51 pm on June 30th) and during the heatwave (i.e. at 3:16 pm on July 2nd). During that period, air temperatures raised from less than 26.6 °C to 33.7 °C (Vilfan et al., 2016). The flight altitude for both flights was 350 m above the ground with a spatial resolution of 0.5 m × 1 m. Different crop types were grown in this area, including three C3 crops (i.e. rapeseed, barley and wheat), already showing signs of senescence, and one C4 crop (corn) still in its growing stage (Fig. 1b, see also ESA report, 2015).

The water limitation case study was conducted on another sugar beet field (50°52′28.45"N, 6°26′58.07″E) close to the city of Julich, Germany. Most parts of the field were in water limitation with clear signs of wilting, while plants in a small area at the corner of the field had sufficient access to water (Fig. 1c). Note this was a long-term effect of reduced water availability because of poor soil, where plants had grown slower, instead of the effect of acute water shortage during a stress event in the strict sense. Airborne imagery was acquired three times to track the diurnal change of the plants, i.e. at 11:50 am, 13:30 pm (solar noon) and 16:05 pm on August 23rd, 2012. The flight altitude was 600 m above ground level, resulting in a spatial resolution of 1 m × 1 m (see also ESA report, 2012).

3.3. Airborne HyPlant data processing

The airborne data were acquired with the HyPlant imaging spectrometer. HyPlant consists of two sensor modules. The DUAL module covers the spectral range from 380 nm to 2500 nm, with a spectral resolution of 3 nm in the visible and near infrared (VNIR) and a 10 nm spectral resolution in the shortwave infrared (SWIR) spectral range. The FLUO module measures radiance in the spectral range from 670 nm ~ 780 nm. It has a fine spectral resolution of full width at half maximum (FWHM) at 0.25 nm and thus enables the retrieval of SIF from the two oxygen absorption bands located at 760 (O_2–A) and 687 nm (O_2–B). A detailed description of the HyPlant sensor and the processing chain can be found in Rascher et al. (2015) and Siegmann et al. (2019).

The improved Fraunhofer Line Discrimination (iFLD) originally introduced by Alonso et al. (2008) was adopted to retrieve SIF at the O_2–A and O_2–B bands from the reflected radiance and emitted fluorescence (Siegmann et al., 2019). In Eq. (1), only far-red SIF and f_{esc} in the NIR band were considered, and thus only the SIF in the O_2–A band at 760 nm was used in this study. All SIF maps shown in this paper thus will be SIF at 760 nm. SIF and NIRvR were both derived from data acquired by the FLUO module of HyPlant. The MODTRAN radiative transfer model was used to atmospherically correct the HyPlant data and retrieve surface reflectance and the upwelling NIR radiance at the bottom of atmosphere simultaneously to get NIRvR (Berk et al., 2005). We deliberately limited the wavelength range for the NIRvR calculation between 675 nm and 775 nm to be consistent with TROPOMI and enable possible conclusions considering the suitability of TROPOMI data for similar analysis. Finally, the narrow-band red surface reflectance (675 nm), NIR surface reflectance (775 nm) and upwelling NIR radiance (775 nm) at the bottom of atmosphere were used to compute NDVI and NIRvR as presented in Eq. (5). To smooth the noise of the hyperspectral data, both the surface reflectance and SIF data were spatially aggregated using a 5 × 5 pixel window for the light adaptation and water limitation case studies. More detailed information about the HyPlant data processing system and data quality can be found in Siegmann et al. (2019).

3.4. Field top-of-canopy measurements

Top-of-canopy SIF, reflectance and upwelling radiance were measured in the field using portable visible and near-infrared spectroradiometers at the light adaptation study site over the sugar beet field. The system included two HR4000 (Ocean Optics, Dunedin, USA) instruments characterized by different spectral ranges and resolutions: the first covering the spectral range 350 nm ~ 1050 nm with a FWHM of 1 nm for reflectance and vegetation indices computation, and the second covering the spectral range 700 nm ~ 800 nm with a FWHM of 0.1 nm for the SIF retrieval. SIF was retrieved in the O_2–A band (760 nm) by means of Spectral Fitting Methods (Cogliati et al., 2015).

The sugar beet targets were measured from nadir at a height above the canopy of 100 cm, corresponding to a circular footprint of about 43 cm diameter. Spectral measurements were acquired after one hour of adaptation to shadow on July 3rd, with similar sky conditions to July 1st, 2015. After the net was taken off, measurements were taken continuously for about twenty minutes with a temporal sampling of about 5 to 15 measurements per minute. Two measurement cycles were acquired, with the first starting at 11:40, and the second at 13:07 local time.

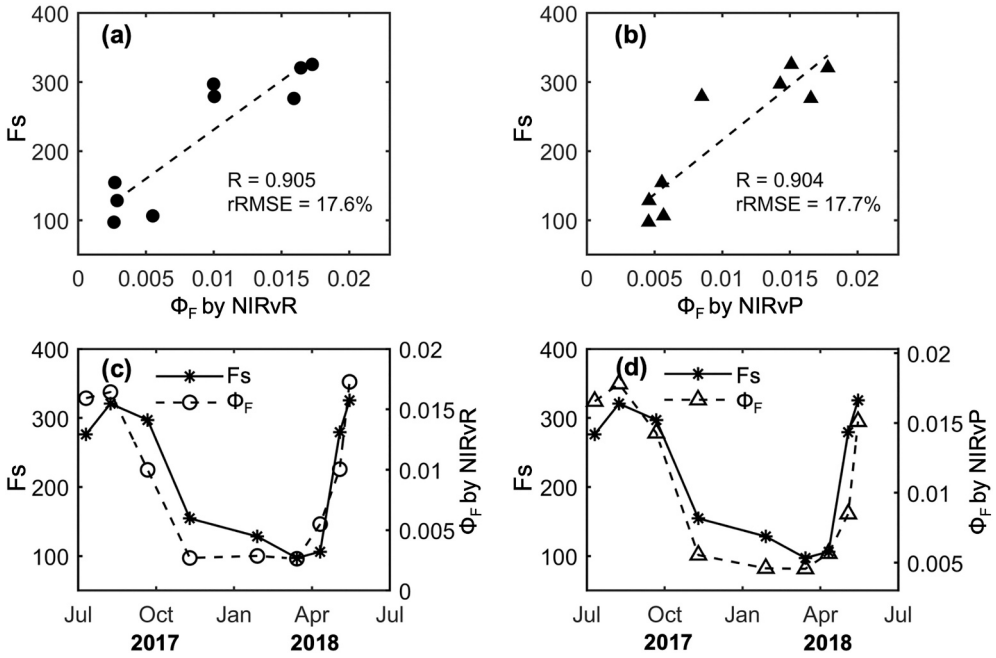

Fig. 2. Comparisons between the NIRvR- (left column) or NIRvP- (right column) derived Φ_F and the leaf-level steady-state fluorescence yield (Fs) measurements at the Niwot Ridge site during 2017– 2018.

3.5. *Field leaf-level measurements*

Leaf-level fluorescence emission was measured at the light adaptation study site over the sugar beet field by means of a FluoWat leaf clip (Van Wittenberghe et al., 2013). A leaf from the top of the canopy was selected, because these leaves were directly observed from the airborne sensor. The leaf was clipped while still beneath the net, and properly pointed to the sun to stimulate photosynthesis in a similar way to natural conditions and representative of the surroundings.

The clip uses a low pass filter that allows the full PAR up to 650 nm to reach the leaf, while cutting out any sunlight that overlaps with chlorophyll fluorescence emission. In this way it is possible to measure the true fluorescence emission spectrum excited by direct sunlight in similar conditions to its neighbors.

An ASD FS3 spectroradiometer with spectral range within 350 nm ~ 2500 nm was coupled to the clip to capture the leaf radiance. The instrument was set to measure continuously at approximately one spectrum per second, capturing the full dynamic of leaf adaptation to increased light once the net was removed. The sequence lasted 10 min.

The acquired fluorescence spectra were normalized according to the radiance measured at 900 nm (no fluorescence, no photoprotection) to compensate for the possible illumination variability, with respect to the first spectrum after the removal of the net, scaling subsequent spectra to make the radiance at 900 nm match the radiance of that first spectrum.

The measurement shows how fluorescence emission suddenly increased when the last portion of the net was removed simultaneously to the airborne sensor overpass, decreasing rapidly right after, and reaching a more slowly steady state after approximately 3 min.

4. Results

4.1. *Results for the evaluation of the NIRvR approach*

The comparison between the NIRvR-derived Φ_F and the measured leaf-level fluorescence yield (Fs) at the Niwot Ridge site showed their strong covariations with high R and low relative Root Mean Square Errors (rRMSEs) (Fig. 2a), indicating that the Φ_F derived by the NIRvR approach can well capture the seasonal variation of the fluorescence yield changes (Fig. 2c). In addition, the NIRvR and NIRvP approaches have led in similar results (Figs. 2b, d).

The SCOPE simulations further supported the evaluation of robustness of the NIRvR approach for estimating Φ_F. Under various vegetation

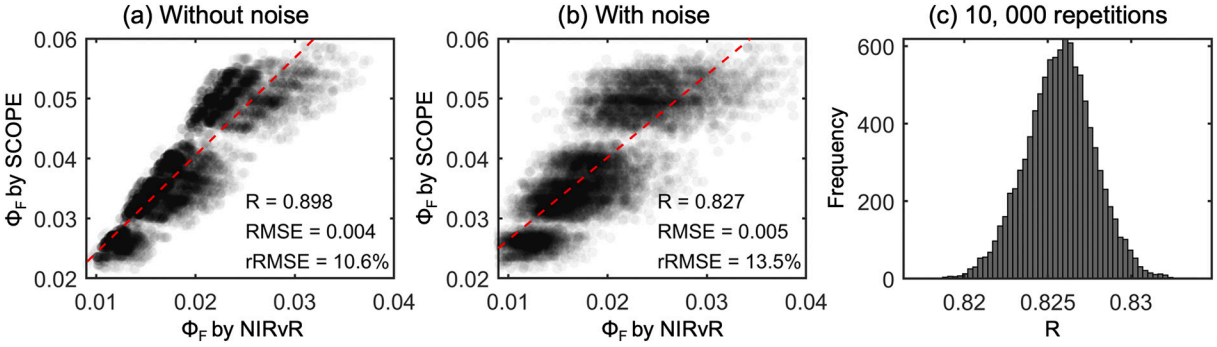

Fig. 3. Evaluation of the NIRvR approach for estimating Φ_F benchmarked with 'true' values from the SCOPE simulations. Data points in (a) are from SCOPE simulations driven by a wide range of soil-leaf-canopy and environmental parameters as summarized in Table S1; (b) shows the results with added observation noises on the simulated SIF and NIRvR; (c) the distributions of R between NIRvR-derived Φ_F and the true values by repeating sampling the noise for 10, 000 times.

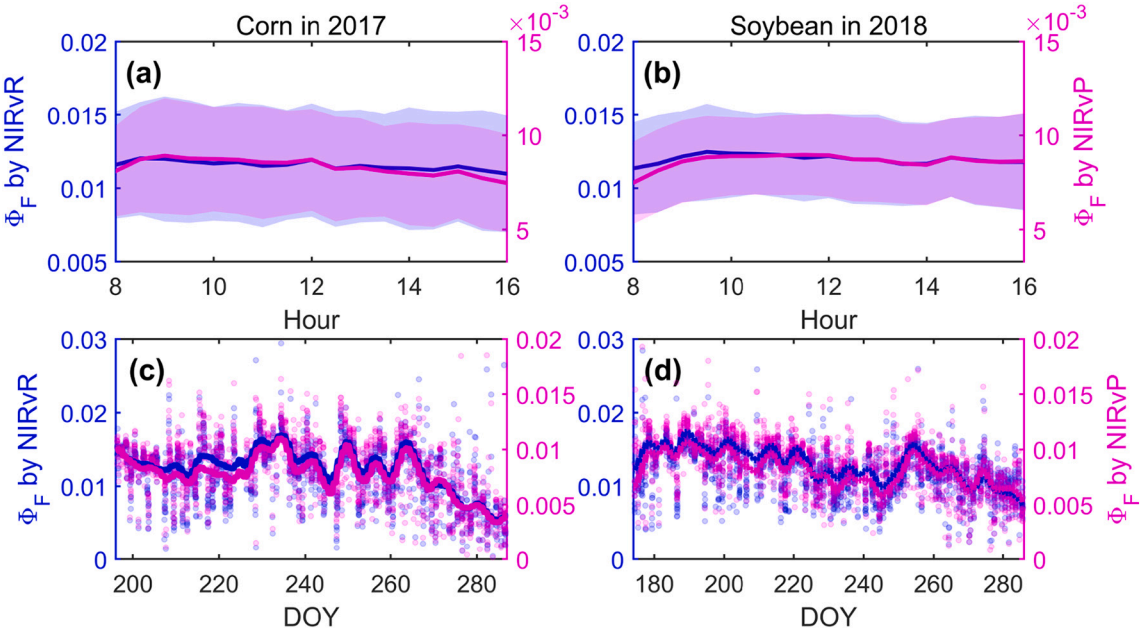

Fig. 4. Comparison between the diurnal (a, b) and seasonal (c, d) variations of the Φ_F estimated by NIRvR and NIRvP at the Nebraska site. Solid lines and shades in (a) and (b) represent the half-hourly Φ_F averaged over the growing season (available days shown in c and d) and the associated standard deviations.

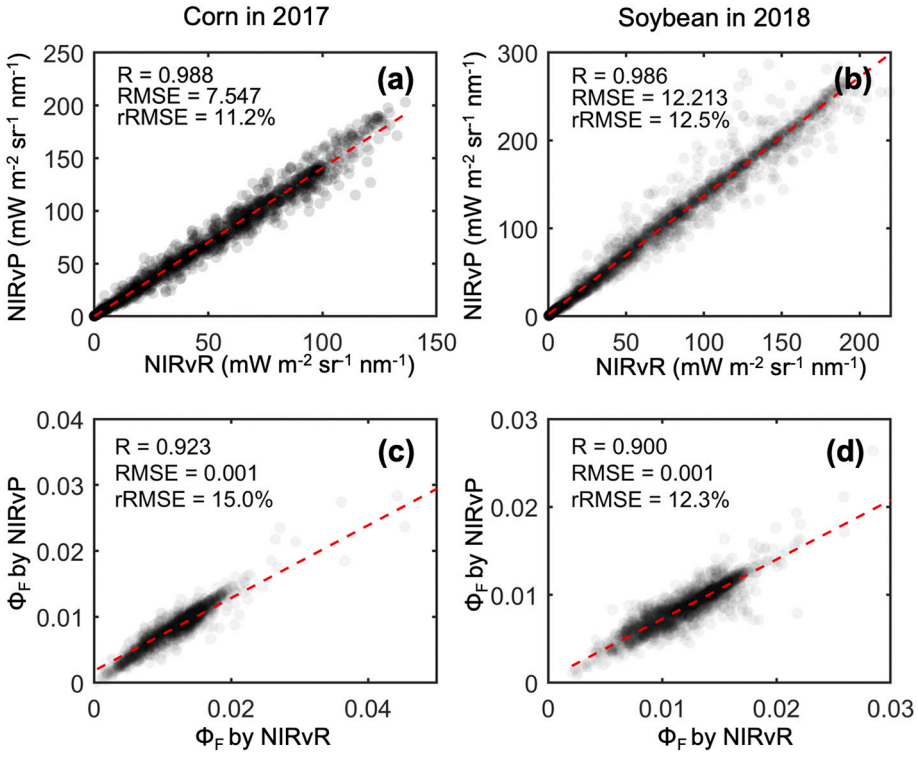

Fig. 5. Comparison between NIRvR and NIRvP, and the Φ_F estimated by them at the Nebraska site.

and environmental conditions (cf. Table S1), the NIRvR approach achieved accurate estimates of Φ_F with a R of 0.898 and a rRMSE of 10.6% (Fig. 3a). Adding noise to the SIF and NIRvR lowered the performance but still resulted in a good agreement, i.e., R = 0.827 and rRMSE = 13.5%, with the R no less than 0.82 in 10, 000 repetitions (Fig. 3c).

At the Nebraska site, the NIRvR approach well reproduced the diurnal and seasonal variations of the NIRvP-derived Φ_F (Fig. 4). Both approaches have resulted in a "bell"-shaped diurnal variation of Φ_F (Figs. 4a, b), and similar trends at the seasonal scale (Figs. 4c, d). The R between NIRvR and NIRvP were both about 0.99 in 2017 and 2018 for the two different crops (corn and soybean), and the rRMSEs were 11.2% and 12.5%, respectively (Figs. 5a, b). The R between the Φ_F derived by NIRvR and NIRvP were also high, which were 0.923 and 0.900, respectively for 2017 and 2018, and the rRMSEs were 15.0% and 12.3% (Figs. 5c, d). These results further suggested that NIRvR could be used as a promising practical and possibly less error prone alternative to the NIRvP to derive and capture the variations of Φ_F at different temporal scales, especially when the simultaneous PAR measurements was not

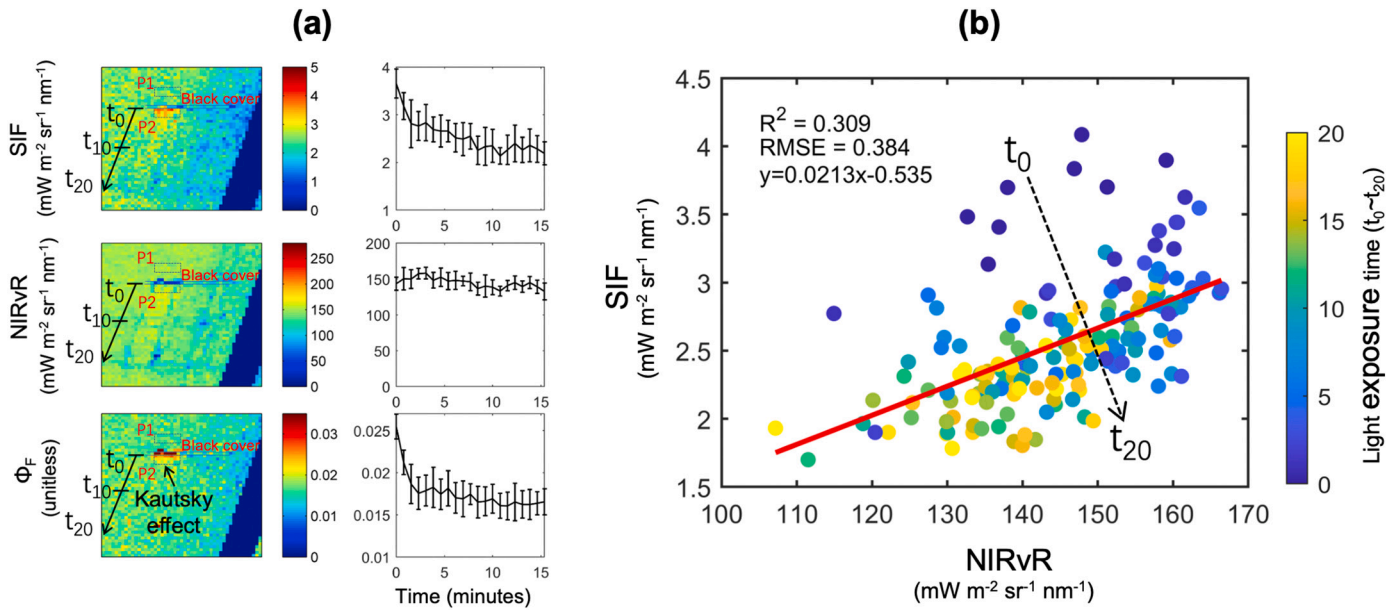

Fig. 6. The spatial distribution and profile in north-south direction for SIF at 760 nm, NIRvR and Φ_F at the light adaptation study site (a) and the corresponding scatterplot (b). The black cover was first removed from the southernmost pixels, meaning light exposure time increased from north (t_0) to south (t_{20}). P2 is the low-light -adapted, stressed area, while P1 is the unaffected neighboring area as the unstressed reference. The profile was calculated when we moved the box of P2 from north to south, and the value was the average of eight transects perpendicular to the north-south direction. The color of the dots in (b) from blue to yellow represents the light exposure time from t_0 to t_{20}, and the red line is the fitted line of all the dots. (For interpretation of the references to color in this figure legend, the reader is referred to the web version of this article.)

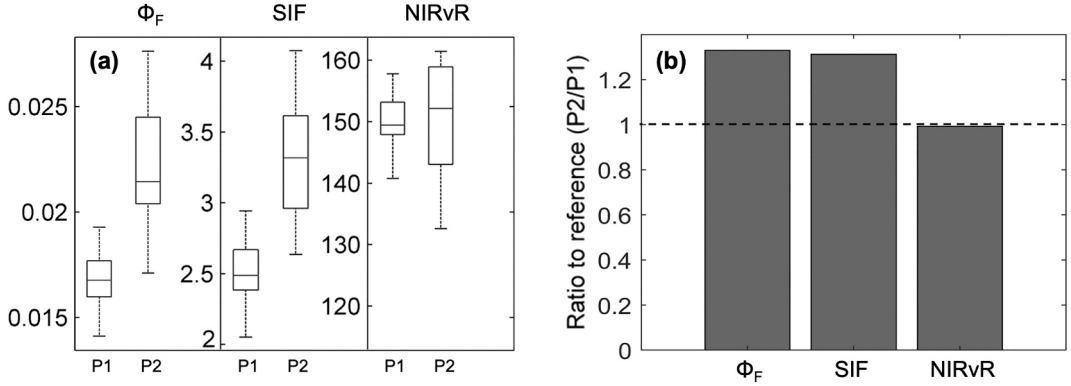

Fig. 7. Distributions of SIF at 760 nm, NIRvR and Φ_F at the light adaptation study site (a), and the ratio of the target area P2 (low-light -adapted, stressed) vs unaffected neighboring area P1 (unstressed reference) (b). SIF and NIRvR are both reported in terms of mW m^{-2} sr^{-1} nm^{-1}. The ratios in (b) were calculated by the average of area P2 and P1 in (a).

available.

4.2. Applications of the NIRvR approach in three case studies

4.2.1. Light adaptation case study

SIF showed the sensitivity to exposure time of low-light -adapted plants to high light. The 50% shading net causing a low-light adaptation of the plants over a relatively large area (from t_0 to t_{20} in Fig. 6a) was continuously removed starting 20 min before HyPlant flights in the south (t_{20}), and ending a few seconds before the flight in the north of the experiment (t_0). The resulting spatial map of SIF (Fig. 6a) shows accordingly the decline of SIF emissions to the process of light adaptation. As can be seen, when the low-light -adapted sugar beet was exposed to high light (t_0), SIF substantially increased and then decreased with time to reach a steady-state level after some minutes.

Unlike SIF, there was no peak nor a gradual decrease found at the same area for the NIRvR. It should be noted that the furled net was still presented in the field as pixels with low NIRvR and SIF values close to the SIF peak, but it was not affecting more than one scan row (around 1 m pixel size). This can cause a slight smearing of the shadowing effect visible in SIF due to mixed pixel effects but the strong increase in SIF is still partially visible.

When investigating Φ_F (i.e., the ratio between SIF and NIRvR) for the light exposure experiment (Fig. 6a), one can clearly see the changing slopes of SIF vs NIRvR with exposure times, while shorter exposure (near t_0) shows larger slopes (Fig. 6b). Quantitatively, there was an obvious difference for the low-light -adapted target area (Patch 2, P2) and the unaffected neighboring reference area (Patch 1, P1) for the median value of the pixels on Φ_F (about 0.022 vs 0.017) and SIF (about 3.3 vs 2.5 mW m^{-2} sr^{-1} nm^{-1}), but not for NIRvR (about 152 vs 150 mW m^{-2} sr^{-1} nm^{-1}). The comparison of the reference (P1) and light adapted canopy area (P2) shows a 30% increase of Φ_F and SIF, while NIRvR does not show obvious changes (Fig. 7).

Fig. 7shows the temporal evolution recording of field-measured top-

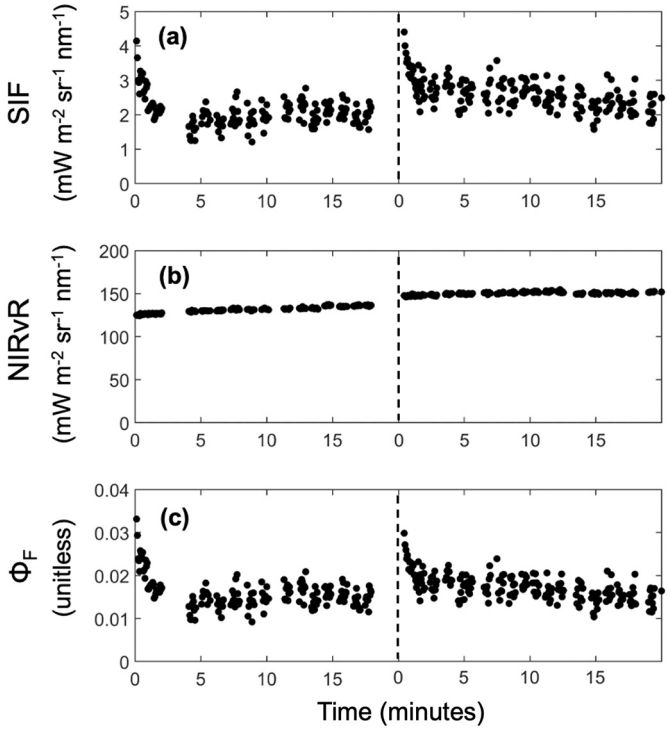

Fig. 8. Variation of ground-measured SIF at 760 nm, NIRvR and Φ_F at top-of-canopy after removing the shadowing net (two cycles) over the sugar beet from the start of the measurement to the end. Two measurement cycles were acquired as described in Section 3.4, with the first starting at 11:40, and the second at 13:07 local time.

of-canopy SIF in the two measurement cycles over the sugar beet crop. Overall, a strong increase in SIF up to 4.5 mW m^{-2} sr^{-1} nm^{-1} can be observed immediately after the exposure to high light conditions for both cycles, followed by a smooth decline towards steady state values after about 50 s (the shadowing effect). This was confirmed also by the Φ_F values, whereas NIRvR did not track the quick dynamics induced by light adaptation (Fig. 7). Overall, this behavior was consistent with results obtained from the HyPlant images in Fig. 6a.

For the leaf-level SIF spectra, once the shading net was removed, the measurements were able to capture the relaxation phases of the Kautsky transient (Fig. 9). However, the spectrometer was not fast enough to capture the fast induction kinetics, but just the maximum fluorescence emission. The measurement series show high fluorescence emission values after the removal of the net and a decrease until the end of the measurements. From the fluorescence emission (Fig. 9), one can see that the fast relaxation transient takes tens of seconds to reach the steady state; thus presenting a dynamic range while achieving a higher maximum fluorescence. Note that the acquired spectra were normalized according to the radiance measured at 900 nm to compensate for the illumination variability. Thus, the normalized SIF emissions in Fig. 9 can well indicate the dynamic variation of Φ_F, which was well captured at the canopy level in Figs. 6~8.

4.2.2. Heat stress case study

For the entire heat stress site (Fig. 10), the relationship between SIF and NIRvR was still strong before (June 29) and during (July 2) the heatwave, with the R^2 values of 0.869 and 0.839, respectively (Fig. 11). The slope of SIF vs NIRvR (in fact Φ_F) decreased from 0.0160 to 0.0146 by about 8.8% (Fig. 11). Different crops reacted differently to heat stress, e.g., while C3 crops including rapeseed, barley and wheat have already shown signs of senescence and the C4 crop (corn) was still in its growing phase (Fig. 10).

On June 29 and July 2, SIF largely decreased in the fields of rapeseed from 1.85 to 1.6 mW m^{-2} sr^{-1} nm^{-1} and wheat from 1.45 to 1.35 mW m^{-2} sr^{-1} nm^{-1}. SIF slightly decreased in the barley field from 1.68 to 1.67 mW m^{-2} sr^{-1} nm^{-1}, while only considerably increased in the corn field (C4 type and still in its growing phase) from 1.15 to 1.35 mW m^{-2} sr^{-1} nm^{-1}.

The variation of NIRvR was similar to SIF while the magnitude was smaller in the other three fields except the barley field (Figs. 6 and 8). NIRvR decreased from 126 to 122 mW m^{-2} sr^{-1} nm^{-1} in the rapeseed field, and from 101 to 97 mW m^{-2} sr^{-1} nm^{-1} in the wheat field, while still increased as SIF from 94 to 104 in the corn field. Unlike the slight decrease in SIF, the barley field had an increase of NIRvR from 114 to 116 mW m^{-2} sr^{-1} nm^{-1}. The increase of NIRvR (Fig. 12) and the decrease of NIRv reflectance in the barley field (Figs. S1-S2) suggest the impact of solar irradiance on NIRvR needs to be considered because the incident NIR irradiance increased from 281.6 to 297.3 mW m^{-2} nm^{-1}.

Φ_F decreased in fields of rapeseed from 0.0150 to 0.0130, barley from 0.0152 to 0.0144, and wheat from 0.0146 to 0.0142 which showed signs of senescence, while slightly increased from 0.0125 to 0.0130 in the corn field which was still in growing from June 30th to July 2nd (Fig. 12). NDVI and NIRv reflectance had similar trends with Φ_F while the relative variation was still different (Fig. S2).

The ratio of Φ_F to reference, calculated as the stressed Φ_F on July 2 divided by the unstressed reference on June 30, was 0.89, 0.95 and 0.98 (<1) in the rapeseed, barley and wheat fields which showed signs of senescence, respectively, while it was 1.03 (>1) in the corn field which was growing. The ratios to reference of SIF and NIRvR had similar trends as Φ_F (above or below one) except at the barley field, where the ratio on NIRvR was larger than one without consideration of the incoming solar irradiance variations from June 30th to July 2nd.

4.2.3. Water limitation case study

The water limitation effect was mixed with the diurnal variation of the incoming solar irradiance and temperature (Fig. 13). For the entire water-limited site, the relationship between SIF and NIRvR was strong for the three acquisition times at 11:50 am, 13:30 pm (solar noon) and 16:05 pm on August 23rd, 2012, with the R^2 of 0.875, 0.921 and 0.926, respectively (Fig. 14). The slope of SIF vs NIRvR (Φ_F) first increased and then decreased from 0.0166 to 0.0204 and 0.0201, respectively. Most parts of the field were in water limitation compared to the small reference corner with sufficient access to water, and the two fields were evaluated separately below.

SIF first increased towards solar noon and then decreased during the afternoon over the water-limited areas from 1.5 to 2.2 and 1.6 mW m^{-2} sr^{-1} nm^{-1}, and over the unstressed reference areas from 1.4 to 1.9 and 1.6 mW m^{-2} sr^{-1} nm^{-1} (Fig. 15).

Similar to the trend of SIF, NIRvR also first increased and then decreased over the water-limited areas from 86 to 102 and 82 mW m^{-2} sr^{-1} nm^{-1}, and over the unstressed reference areas from 97 to 112 and 89 mW m^{-2} sr^{-1} nm^{-1} (Fig. 15).

Φ_F also showed this trend from 0.017 to 0.021 and 0.020 over the water-limited area (Fig. 15), while it increased monotonously in the morning towards noon time from 0.014 to 0.018 and 0.019 over the unstressed reference areas, with high temperature and high light at noon. Φ_F remained high due to still high temperatures but less light in the afternoon.

For the ratio of the water-limited area divided by the unstressed reference, both SIF and Φ_F had a similar diurnal pattern. The ratio of SIF first increased from 1.08 to 1.12 and then decreased to 1.00, the ratio of Φ_F first increased from 1.19 to 1.23 and then decreased to 1.09. However, the ratio of NIRvR was nearly constant at 0.92 over the three acquisition times. The ratios of NIRvR was always smaller than one, while the ratio of SIF and Φ_F were always larger than one (Fig. 15), suggesting that the water-limited sugar beet has a higher Φ_F than the unstressed reference under the light and temperature condition in this study.

In this case study, NDVI and NIR reflectance showed opposite diurnal

Table 1
Characteristics and data pre-processing procedures needed for several SIF and NIRv-related indicators to detect effects of abiotic changes and stresses without the reference fields in the same image.

Remote sensing indicators	Information conveyed	Need incident solar irradiance normalization?	Need sun-sensor geometry correction?	Sensitive to soil background brightness?
SIF at 760 nm	PAR, canopy structure ($FPAR_{chl}$, f_{esc}), leaf physiology	Yes	Yes	No
NDVI	Canopy structure ($FPAR_{chl}$), leaf optics	No	Yes (but not as necessary as SIF and NIRv)	Yes
NIR	Canopy structure ($FPAR_{chl}$, f_{esc})	No	Yes	Yes
NIRv (NDVI×NIR)	Canopy structure ($FPAR_{chl}$, f_{esc}), leaf optics	Yes (Just transform NIRvR to get normalized NIRv reflectance)	Yes	Slightly (Slightly more sensitive than SIF, but less sensitive than NIR and NDVI)
NIRvR (NDVI×NIRrad)	Solar irradiance, canopy structure ($FPAR_{chl}$, f_{esc}), leaf optics	Yes	Yes	Slightly
SIF/NIRvR (Φ_F)	Leaf physiology	No	No (if the same sensor is used for SIF and NIRvR)	Slightly

trends due to different impacts of shadows in view by solar angle variations, while the magnitude of the NDVI variation was much smaller compared to NIR (Figs. S3 and S4). NIRv had similar but smaller diurnal variation compared to NIR. Considering the ratio of the stressed area to the unstressed reference, NIRv was less than one, while NIR was close to one (Fig. S4).

5. Discussion

Several previous studies on the stress response of SIF either did not account for the canopy structure effect and sun-sensor geometry, especially f_{esc} (Wen et al., 2020; Wieneke et al., 2018; Wohlfahrt et al., 2018; Yoshida et al., 2015), or required the corresponding simultaneous PAR product as the input parameter (Wang et al., 2020; Siegmann et al., 2021), which may lead to uncertainties or challenges in interpreting SIF's responses to environmental changes and stresses. We showed the mechanistic linkage between SIF and NIRvR in Eq. (1), compared the differences between SIF and NIRvR in response to three extreme environmental conditions, and evaluated the Φ_F variability estimated by SIF/NIRvR in Eq. (2). We found clear evidence that SIF and Φ_F were more sensitive to light adaptation status and abiotic stresses compared to NIRvR. Also, we found that isolating Φ_F can help to more clearly see physiological stress effects that are not superposed to structure-related effects. A more detailed discussion will be in the below subsections about the comparison of several SIF and NIRv-related indicators on the characteristics and data pre-processing procedures needed for detecting the effects of abiotic changes, the possible compounding effects in leaf-canopy decoupling, and the uncertainties in canopy-scale Φ_F extraction and stress detection.

5.1. Characteristics of SIF- and NIRv-related indicators for detecting plant response to abiotic changes and stresses

Isolating the physiological information contained in Φ_F can have advantages for vegetation monitoring. As shown in Table 1, SIF is a mixed signal which can be affected by many factors, e.g., PAR, sun-sensor geometry, canopy structure and leaf physiology. Through Φ_F estimated via SIF/NIRvR, we can have a clear understanding of the response of leaf physiology to stress, which is minimally affected by the diurnal or seasonal variation of PAR, sun-sensor geometry and canopy structure. Apart from the advantages of being able to clearly attribute changes in SIF to different factors, in some cases, Φ_F can be more sensitive to vegetation stress than SIF. For example, in the case of water stress, canopy structure effects as captured by NIRvR went into opposite directions as the physiological responses (the ratio to reference <1 for NIRvR but the ratio >1 for Φ_F in Fig. 15d), which decreased the sensitivity of SIF to stress. Also, isolating Φ_F from canopy-scale SIF observations is important for the plant physiologists whose interest is at the leaf scale to detect stress. In the case of light adaptation and heat stress, SIF and Φ_F had similar relative responses (Figs. 3 and 8), but isolating Φ_F revealed that heat stress responses were a combination of physiological and structural factors, which is consistent with the findings of Xu et al. (2021). It is also notable that SIF responses can be misinterpreted if the physiological and structural factors are not disentangled. For example, Siegmann et al. (2021) found that the diurnal hysteresis of some crop types was unexpectedly not due to physiological but structural factors.

One of the advantages of using SIF/NIRvR to approximate Φ_F to detect effects of abiotic changes is that there is no need to require PAR as the input parameter. As long as SIF and NIRvR are acquired from the same sensor or with the same sun-sensor geometry and ratio of diffuse radiation, the impacts of incident solar irradiance (PAR), canopy structure and sun-sensor geometry (influences $FPAR_{chl}$ and f_{esc}) can be directly cancelled by their ratio. Thus Φ_F can be extracted by only the canopy-scale SIF and NIRvR observations without any additional measurements. The potential geometric correction and spatial resolution mismatches between SIF and NIRvR can be minimized if they are from the same sensor, such as the HyPlant FLUO module in this study. The use of SIF/NIRvR also enables large-scale applications with TROPOMI measurements because of the potential of TROPOMI (675 nm ~ 775 nm) to extract SIF and NIRvR simultaneously. However, atmospheric correction is the key to acquire the surface reflectance and the upwelling NIR radiance. Note that the shape of the downwelling solar irradiance spectrum at the bottom of atmosphere can lead to the varying ratio of INIR to PAR in Eqs. (1–2), which can lead to the deviations between NIRv reflectance times PAR (NIRvP = NIRv×PAR) and NIRvR. This spectrum shape is determined by different atmospheric scattering effects at different wavelengths, which can be impacted either by the varying sky conditions from sunny days to cloudy days with different ratio of diffuse radiation, or by different solar zenith angles at different latitudes and times of the day.

Instead of solely relying on Φ_F for stress detection, we recommend the combined use of illumination and angular normalized SIF and NIRv, together with Φ_F, to make complementary contributions to detect effects of abiotic changes. Note that Φ_F primarily contains leaf physiology information, while abiotic changes may lead to symptoms of canopy structure and leaf optical property variations (Figs. S2 and S4). We summarized the characteristics of the information conveyed in SIF and optical VIs (Table 1). Note that NIRv reflectance can be described by the product of NDVI times NIR reflectance, in which NDVI is more sensitive to chlorophyll content over dense canopies (Gamon et al., 1995), and NIR is more sensitive to the leaf inclination angle. Both chlorophyll content and leaf inclination angles are known to respond to abiotic changes and stresses, although the responses may be slower (Sanchez et al., 1983). Leaf angle changes can go in either way, either more erectophile/curling to avoid strong light by minimizing absorption, or drooping when they lose a lot of water (Lonbani and Arzani, 2011; Werner et al., 1999). Thus SIF and NIRv with mixed information of canopy structure and leaf physiology are possible to have either similar or opposite trends with Φ_F on the response to stress, and especially the latter situation highlights the value of Φ_F on stress detection in practice.

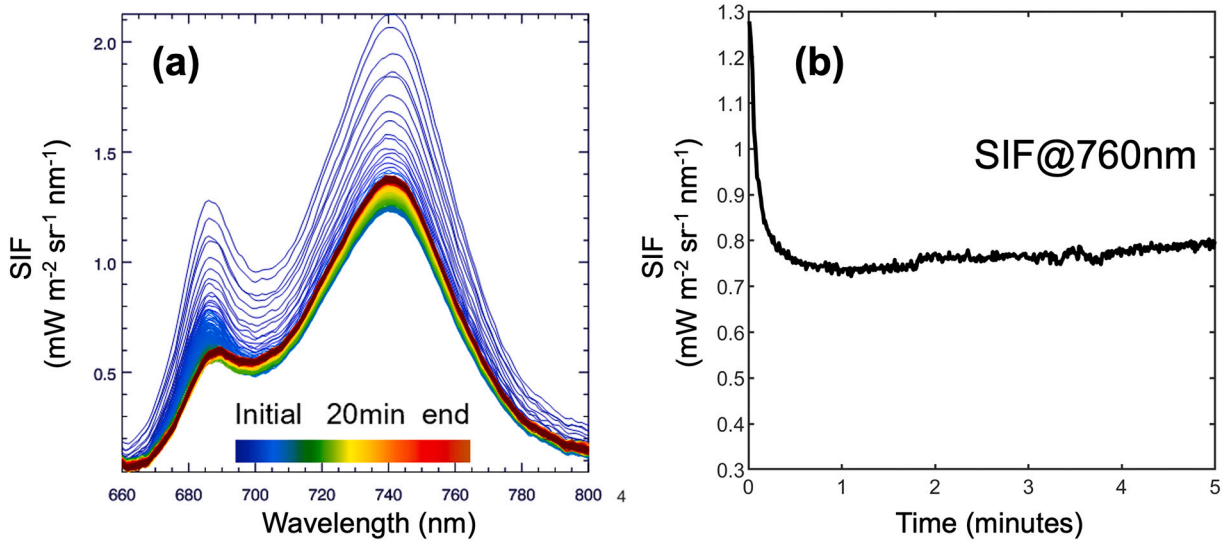

Fig. 9. Dynamics of the leaf-level fluorescence emission spectra (a) and of SIF at 760 nm (b), from the start of the measurement (t_0 in blue) to the end (t_{20} in dark red) (Modified from ESA report, 2015). For (b), only the main variation period of the first five minutes was displayed. Note the fluorescence spectra were normalized according to the radiance of the first measurement through the radiance measured at 900 nm to compensate for the possible illumination variability. (For interpretation of the references to color in this figure legend, the reader is referred to the web version of this article.)

Using a reference area is important to detect the effects of abiotic changes, but it can be challenging in practice to obtain such a reference. If the reference is from the same fields as the treatment or stress exposure, as in the case of the water-limited site in this study, the same incident solar irradiance and sun-sensor geometry information conveyed on SIF can be cancelled by the ratio of the water-limited area to the reference. However, especially for satellite-based stress detection, the simultaneous unstressed reference is usually unavailable, while periods from neighboring years, days or even hours have served as the reference (Sun et al., 2015; Wen et al., 2020). Normalizing SIF by PAR is needed for stress detection to avoid the impact of the PAR variation, e.g., the variation of SIF in Fig. 15 was mostly due to the diurnal PAR changes. Fortunately, for a given target area, if satellites can have similar revisit time of a day, SIF observations are possible to have similar PAR and sun-sensor geometry for the time-series analysis in a few days or at the same date of neighboring years. For the diurnal, seasonal and cross-sensor analysis, the possible PAR and sun-sensor geometry mismatch may need to be considered prior to SIF applications on the effects of abiotic changes and stresses detection. The diurnal variation of Φ_F can complicate the application for stress detection, unless there is an unstressed reference area as in Fig. 15, or there are unstressed reference observations at the same time of a day with similar environmental factors on a nearby date.

5.2. Compounding effects in leaf-canopy decoupling

We found that Φ_F can either increase or decrease under environmental changes and stresses. Φ_F increased in the light adaptation site due to the shadowing effect (Fig. 6a), but decreased in the heat stress at the rapeseed, barley and wheat fields (Fig. 12). The leaf-scale measurements clearly showed SIF after sudden illumination rapidly declined from the peak in response to the build-up of photoprotection, and then rose again when excessive non-photochemical quenching (NPQ) was slowly relaxed or chloroplast movements slowly modified the fraction of absorbed light and SIF emission (Fig. 9). Such an effect was not visible neither in the Hyplant (Fig. 6a) nor in the field measurements at the top of the canopy (Fig. 8). Such a discrepancy between the leaf-scale and canopy-scale could be caused by different sensitivity of the instrumentation, the natural variability within the canopy, the structural changes in the canopy, e.g., by paraheliotropic movements of the leaves, or a superposition of the above effects.

The response of Φ_F to water limitation is complex and still remains incompletely understood. We did not see the decrease of Φ_F in our case study of long-term reduced water availability under high light. Under severe water limitation, the sink provided by photochemistry tends to zero, NPQ reaches a maximum and as a consequence, fluorescence emission can also increase. This is actually the time when the light-harvesting complexes (LHCs) no longer can be protected and start to be damaged irreversibly. In this study, plants had grown slower due to the long-term reduced water availability in the water-limited area of the field. This is different from acute drought stress, where well-grown plants having the same developmental stage are suddenly exposed to drought stress, which causes an acute (physiological) stress response, i.e. stomatal closure and down regulation of photosynthesis. For example, Φ_F has been observed to both increase and decrease in previous studies on acute drought stresses. The basis of these divergent effects is not clear, and the divergent explanations that have been offered are as below. A few previous studies show that canopy-scale apparent SIF yield (which is different from Φ_F) declines under acute drought stress possible due to the stomatal closure and decreased Calvin cycle activity (Ač et al., 2015; He et al., 2020; Wen et al., 2020). However, recent progress indicates it is not strange to observe the increase of Φ_F even during the drought stress, as the three recent case studies summarized in Table 1 in Jonard et al. (2020). Besides, note that at the canopy scale, even under high light illumination, there are still a considerable proportion of shaded leaves being exposed to low light intensity, especially for dense canopies. Chen et al. (2019) found that Φ_F may still increase under drought stress and low light, due to the competitive relationship between SIF and NPQ with photosynthesis. Their explanation is that more photosynthetic reaction centers are closed, which leads to the inhibition of photochemical quenching and the increase of fluorescence (Baker, 2008); in addition, electron and light energy are excessive under drought stress, and non-photochemical quenching and fluorescence are utilized to consume the excessive light (Chen et al., 2019). van der Tol et al. (2014) also found that Φ_F may increase with stress under both high light and very low light in their Fig. 7, because stress reduces the photosynthetic yield; in addition, the yield of NPQ increases, and at a certain point, NPQ is so large that it causes a stagnation of Φ_F. This process is reversed with decreasing stress. In summary, Φ_F can either increase or decrease with increasing stress, depending on the severity of

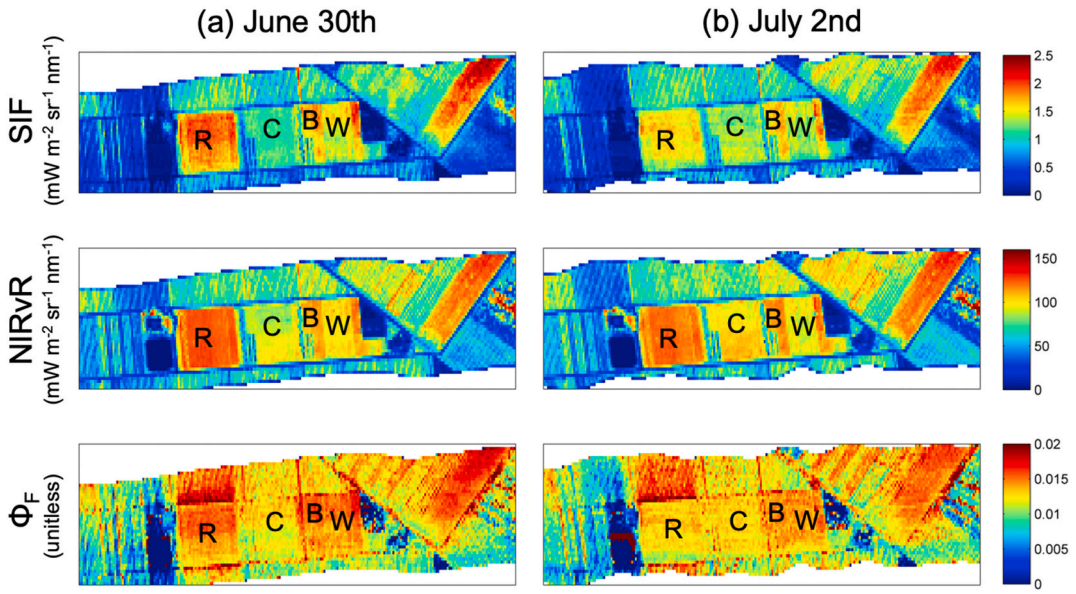

Fig. 10. The spatial distribution of SIF at 760 nm, NIRvR and Φ_F at the heat stress study site before the heatwave at 3:51 pm on June 30th, 2015 with the air temperature no more than 26.6 °C (a) and during the heatwave at 3:16 pm on July 2nd, 2015 with the air temperature reaching 33.7 °C (b). The incident NIR irradiance slightly increased from 281.6 to 297.3 mW m^{-2} nm^{-1}. The R, B and W represent three C3 crops: Rapeseed, Barley and Wheat, and C represents one C4 crop: Corn.

stress, the light intensity, the temperature and the related regulation of NPQ (e.g., see Fig. 1d in Magney et al. (2020)). In order to detect such changes in Φ_F, the effect of canopy structure changes must be removed from satellite SIF observations.

This suggests for the water limitation detection, it is necessary to take the concurrent environmental factors into account, and the trend of Φ_F in water limitation still needs further leaf-scale quantitative and comprehensive analysis. For the water limitation detection, it is recommended to use imageries in neighboring days but at the same time of a day as the unstressed reference, to avoid the possible diurnal varying factors such as the incident solar irradiance and temperature.

Variation of leaf physiology (i.e. Φ_F) and canopy structure (e.g., leaf inclination angle) under abiotic changes could have opposite impacts on SIF, e.g., Φ_F is increasing while NIRv is decreasing, such that the two effects partially counteract one another, and eventually SIF is decreasing under abiotic changes (Figs. 11 and S4). This opposing effect can reduce the sensitivity to detect effects of abiotic changes by only the canopy-scale SIF observations, and suggests the necessity to combine the canopy-scale SIF and NIRvR to decouple the leaf physiology and canopy structure contribution. The canopy structure can behave differently according to the degree and duration of the environmental constraints. For the long-term effects of reduced water availability, vegetation can develop differently throughout the season and have a different canopy structure with sparser canopy, while acute drought stress may cause changes in leaf inclination (droopy leaves) or even leaf droppings when turgor loss occurs above wilting point. In our site with severe water limitation conditions, there was a major wilting leading to a substantial structural change in the canopy, and the leaves also did loose turgor to a great extent and the shape of the canopy changed a lot from mostly erectophile to planophile (Fig. S5), while the reference area was much better as they had access to sufficient water.

5.3. Uncertainties in canopy-scale Φ_F extraction and abiotic change and stress detection

The direct validation of canopy-scale Φ_F remains to be challenging. There is usually a scale mismatch between leaf SIF (in a few centimeters) and remotely sensed canopy SIF ($\geq$1 m with sunlit/shaded leaves under different light intensity for each leaf) to draw scatterplots. Significance test was conducted to evaluate whether the Φ_F under stress is significantly different from that under no stress. A *t*-test was conducted with the null hypothesis (H_0)—the Φ_F of the stress and unstressed areas are equal ($\mu = \mu_0$), and the alternative hypothesis (H_1)—the Φ_F of the stress and unstressed areas are not equal ($\mu \neq \mu_0$). For all the three case studies (Fig. 7a, Fig. 12c and Fig. 15c), the *t*-test result fell in the rejection region at the 5% significance level, and thus the test rejects the null hypothesis. Meanwhile, all of the *p*-values were less than 0.001, which suggests that there was overwhelming evidence to support the alternative hypothesis H_1 that the Φ_F of the stress and unstressed areas were significantly different.

The uncertainties in the canopy-scale Φ_F estimation by simultaneous SIF and NIRvR observations include the accuracy of the SIF retrieval and the approximation of the true NIR radiance of vegetation by the product of NDVI times the upwelling NIR radiance. Although generally NIRv by NDVI×NIR is a good approximation of NIR reflectance of vegetation over a black soil background, there can still be some overestimation at low vegetation density and underestimation at high vegetation density, because the soil NDVI is not zero and the NDVI at dense canopy is still less than one (Zeng et al., 2019). This leads to the non-zero offset (Figs. 7 and 10), which means pixels with zero SIF values can have non-zero NIRvR. Thus the absolute value of Φ_F by their slope could be impacted, although this can partly be accounted for with the regression intercept. Fortunately, the abiotic change detection is more based on the time-series analysis, and thus the temporal trend of Φ_F is more important than the absolute value. The more accurate estimation of the true NIR radiance or reflectance of vegetation over a black soil background still needs exploration. The influence of the solar zenith angle and vegetation shadows on the Φ_F estimated by SIF/NIRvR have been implicitly considered, because SIF and NIR photons by vegetation have the similar f_{esc} and shadowing effect (Yang et al., 2019; Zeng et al., 2019). Besides, this influence can be minimized when we have the unstressed reference area in the same image and calculate the ratio of the stressed area to the unstressed reference (Figs. 3, 8 and 11).

SIF, NIRv and NDVI derived from airborne images in this study were not angular normalized in the standard sun-sensor geometry, because multi-angular observations were rare for the airborne platform, while

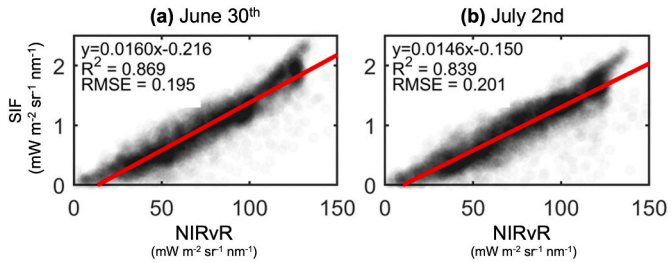

Fig. 11. The scatterplot between SIF at 760 nm and NIRvR at the heat stress study site before the heatwave at 3:51 pm on June 30th, 2015 (a) and during the heatwave at 3:16 pm on July 2nd, 2015 (b).

satellite platforms could have more sufficient multi-angular observations. The opposite trends for the diurnal variation of NDVI and NIRv (or NIR) (Fig. S4) were mostly due to the diurnal variation of the solar zenith angle, with shadows increased NDVI but decreased NIRv (or NIR) (Kaufmann et al., 2000). Using satellite SIF and surface reflectance multi-angular observations for the sun-sensor geometry correction of SIF also needs further exploration, as a pre-processing step of the SIF applications (Hao et al., 2021; He et al., 2017; Zhang et al., 2018; Zeng et al., 2019) on the effects of abiotic change detection. Exploring the Photochemical Reflectance Index (PRI) vs Φ_F relationship under various stress conditions is also a promising direction, while the downscaling of PRI from the canopy to leaf scale (or angular correction) for the HyPlant data without multi-angular observations (Siegmann et al., 2019) is challenging and still deserves investigations for the further PRI vs Φ_F analysis.

Finally, the response of Φ_F was quite diverse depending on abiotic changes and crop types. If Φ_F changes, it is challenging to determine which abiotic change happens without sufficient prior information about the crop type and environmental conditions. Thermal imageries in combination with SIF and hyperspectral dataset could therefore be helpful for airborne-based detection of effects by abiotic changes. Besides, there are many abiotic factors that can change Φ_F. How Φ_F changes with concurrent abiotic factors (e.g., water and temperature together), and how to disentangle the different abiotic changes separately from the mixed signal of Φ_F variation still need further exploration. Furthermore, Liu et al. (2017) found that Φ_F is weakly sensitive to the photosynthetic pathway type, while there is large difference in the light use efficiency between C3 and C4 crops. This means in the comparison of SIF-GPP slopes across plant species, the differences between the C3 and C4 species should be considered.

6. Conclusions

We conclude that normalizing SIF by NIRvR provides an efficient strategy to normalize SIF to canopy structure, and extract the canopy-scale Φ_F variation. The performance of the proposed NIRvR approach was evaluated with field data, modeling experiments and the results by using the NIRvP approach. NIRvR-derived Φ_F can well capture the seasonal variation of the fluorescence yield changes, and well reproduced the diurnal and seasonal variations of the NIRvP-derived Φ_F. Φ_F derived from HyPlant image data clearly showed sensitivity to a physiological response caused by dynamics of abiotic drivers, including light, temperature and water availability. We particularly highlight the observed SIF and Φ_F response to dynamically changing light environments (the shadowing effect), while greenness-based vegetation measures (NIRvR) do not. This provides an additional proof on the

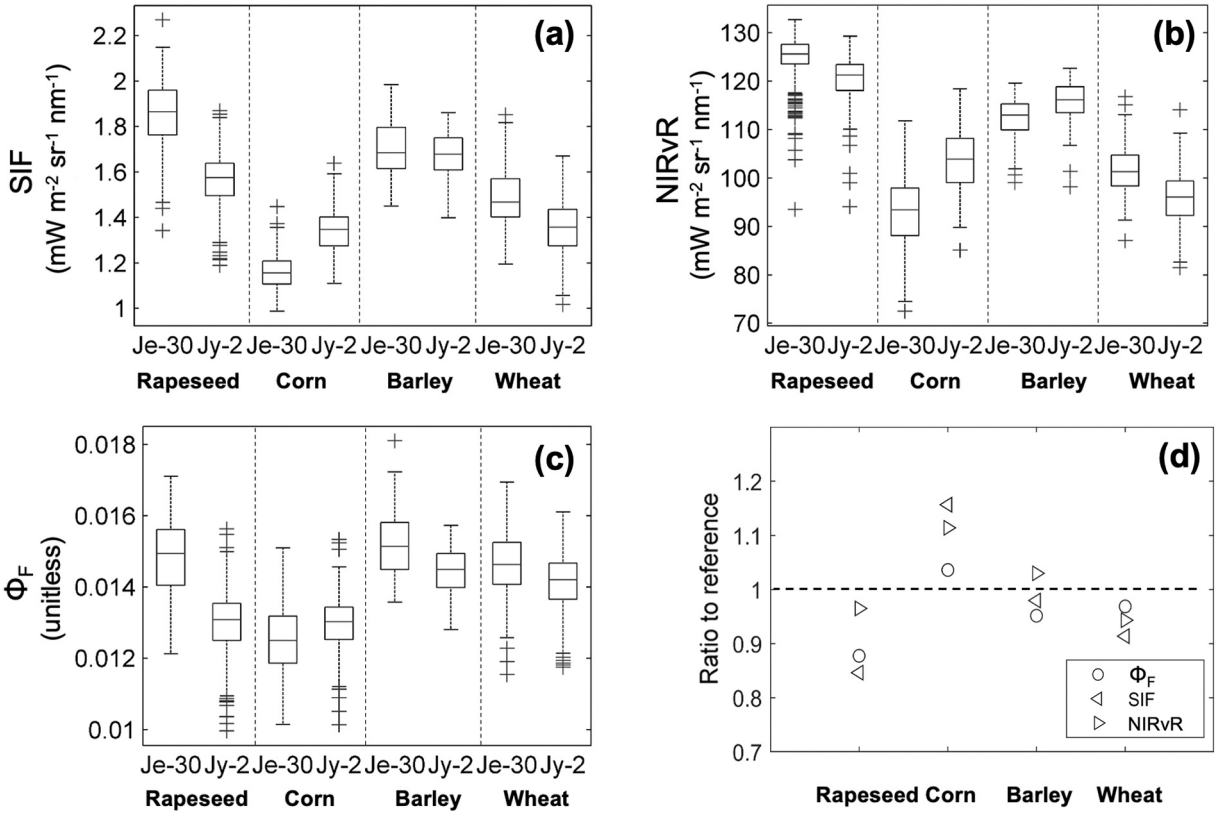

Fig. 12. The boxplots of SIF at 760 nm (a), NIRvR (b) and Φ_F (c) at the heat stress study site at the Rapeseed, Barley, Wheat and Corn fields. Je-30 represents June 30th, 2015 before the heatwave at 3:51 pm, while Jy-2 represents July 2nd, 2015 during the heatwave at 3:16 pm. The ratios in (d) were calculated as the average of the stressed values (during the heatwave) divided by the average of the unstressed reference (before the heatwave) of each field. The error bars in (a-c) represent the variability of the pixels within the patches.

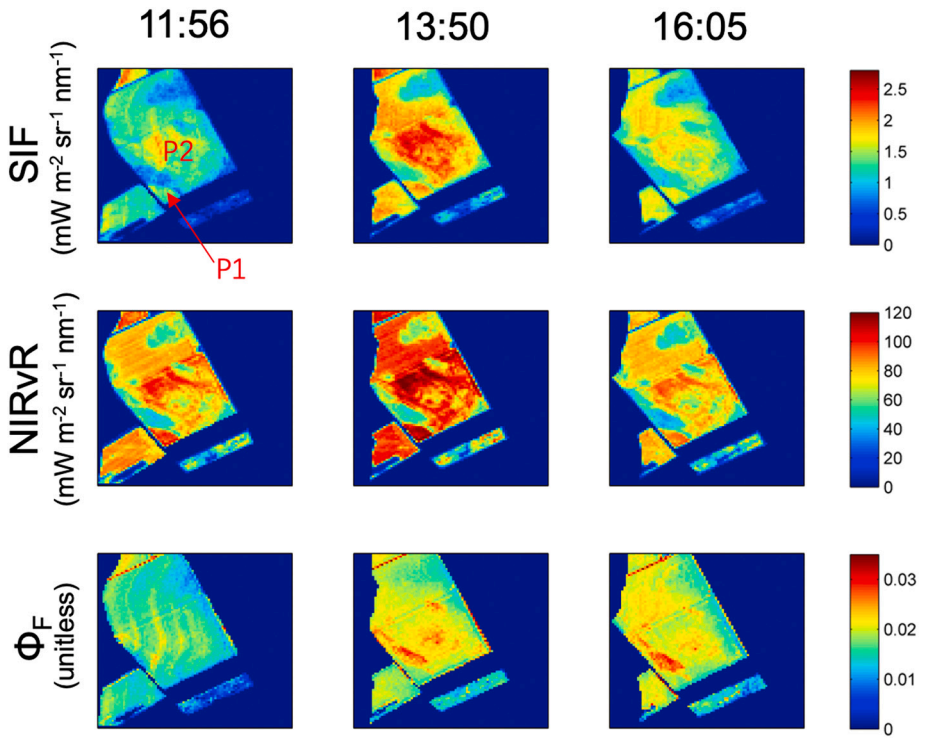

Fig. 13. The spatial distribution of SIF at 760 nm, NIRvR and Φ_F over the water limitation study site at 11:50 am, 13:30 pm (solar noon) and 16:05 pm on August 23rd, 2012. The incident NIR irradiance at 11:50 am, 13:30 pm and 16:05 pm was 255.7, 278.0 and 230.8 mW m^{-2} nm^{-1}, respectively. P2 is the water-limited area in the field (Patch 2), while P1 is the small unstressed reference area with sufficient access to water at the corner of the field (Patch 1).

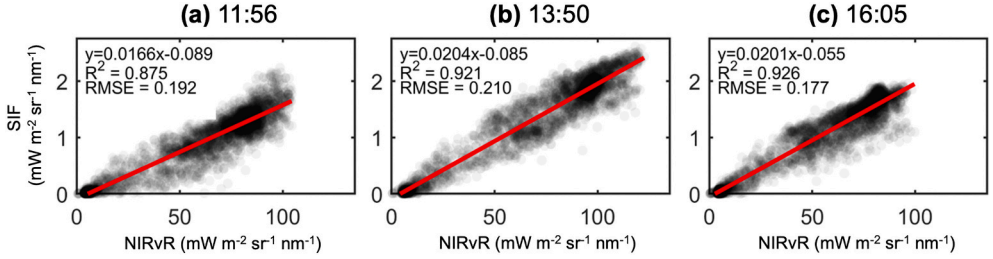

Fig. 14. The scatterplot between SIF at 760 nm and NIRvR at the water limitation study site at 11:50 am, 13:30 pm (solar noon) and 16:05 pm on August 23rd, 2012.

complementarity of SIF compared to common remote sensing measures. Our proposed approach to derive Φ_F offers several advantages for plant stress detection compared to existing strategies. Since SIF and NIRvR share the same sun-sensor geometry, there will be no mismatch on geometric correction and spatial resolution, and normalizing SIF with NIRvR results in a sensitive stress proxy Φ_F not affected by canopy structure and sun-sensor geometry (f_{esc}). Another advantage of the proposed approach is that corresponding PAR (400 nm ~ 700 nm) products, typically required to normalize SIF, are not needed here. This opens the space of opportunities to extract Φ_F even from sensors that do not have corresponding simultaneous PAR and $FPAR_{chl}$ products to calculate APAR, and only sample a smaller spectral window, e.g., TROPOMI (675 nm ~ 775 nm). With SIF as an instantaneous measure and NIRvR as a reference for canopy structure, one can detect stress symptoms at much shorter time scales than a slow reacting radiance-based NIRvR.

CRediT authorship contribution statement

Yelu Zeng: Conceptualization, Methodology, Formal analysis, Writing – original draft, Writing – review & editing. **Min Chen:** Conceptualization, Methodology, Writing – original draft, Writing – review & editing. **Dalei Hao:** Methodology, Writing – original draft, Writing – review & editing. **Alexander Damm:** Methodology, Formal analysis, Data curation, Writing – review & editing. **Grayson Badgley:** Conceptualization, Methodology, Writing – review & editing. **Uwe Rascher:** Data curation, Writing – review & editing. **Jennifer E. Johnson:** Writing – review & editing. **Benjamin Dechant:** Writing – review & editing. **Bastian Siegmann:** Data curation, Writing – review & editing. **Youngryel Ryu:** Methodology, Writing – review & editing. **Han Qiu:** Writing – review & editing. **Vera Krieger:** Data curation, Writing – review & editing. **Cinzia Panigada:** Data curation, Writing – review & editing. **Marco Celesti:** Data curation, Writing – review & editing. **Franco Miglietta:** Data curation, Writing – review & editing. **Xi Yang:** Writing – review & editing. **Joseph A. Berry:** Conceptualization, Methodology, Writing – review & editing.

Declaration of Competing Interest

The authors declare that they have no known competing financial interests or personal relationships that could have appeared to influence the work reported in this paper.

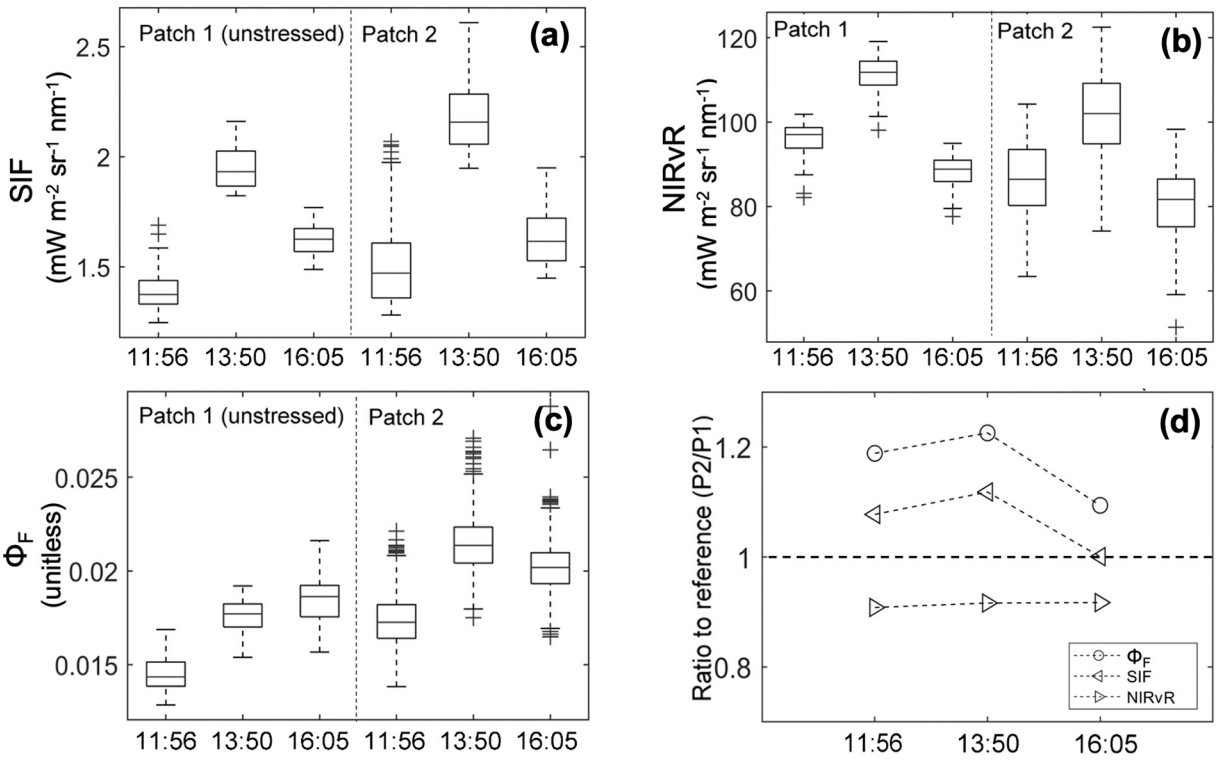

Fig. 15. The boxplots of SIF at 760 nm (a), NIRvR (b) and Φ_F (c) at the water limitation study site at 11:50 am, 13:30 pm (solar noon) and 16:05 pm on August 23rd, 2012, and the ratios which were calculated as the average values for the water-limited area (Patch 2, P2) divided by those for unstressed reference area (Patch 1, P1) with sufficient access to water (d). The error bars in (a-c) represent the variability of the pixels within the patches.

Acknowledgement

This research was supported by the National Aeronautics and Space Administration (NASA) through Remote Sensing Theory and Terrestrial Ecology programs 80NSSC21K0568 and 80NSSC21K1702 granted to Min Chen. Y. R. was supported by National Research Foundation of Korea (NRF-2019R1A2C2084626). The authors thank Luis Alonso at University of Valencia for providing the leaf-level dataset and having fruitful discussion. We thank Tiziana Speckert for collecting information of the three case studies. We thank Kaiyu Guan, Genghong Wu and Troy Magney for providing the SIF field datasets in the evaluation. Airborne acquisition and data analysis were financed by the European Space Agency (ESA) in the frame of the HyFLEX campaign (ESA contract No. 4000107143/12/NL/FF/If), the SoyFlex 2015 campaign (ESA contract No. 4000107143/12/NL/FF/If CCN3), and the Photoproxy campaign (ESA contract No. 4000125731/19/NL/LF). Additional support to the field data acquisition was provided by the SFB/TR 32 "Patterns in Soil-Vegetation-Atmosphere Systems: Monitoring, Modelling, and Data Assimilation"—subproject D2 (www.tr32.de), funded by the Deutsche Forschungsgemeinschaft (DFG). Part of this work was performed within the German-Plant-Phenotyping Network which is funded by the German Federal Ministry of Education and Research (project identification number: 031A053) and was supported by Campus Klein-Altendorf of Bonn University.

Appendix A. Supplementary data

Supplementary data to this article can be found online at https://doi.org/10.1016/j.rse.2021.112856.

References

Ač, A., Malenovský, Z., Olejníčková, J., Gallé, A., Rascher, U., Mohammed, G., 2015. Meta-analysis assessing potential of steady-state chlorophyll fluorescence for remote sensing detection of plant water, temperature and nitrogen stress. Remote Sens. Environ. 168, 420–436.

Alonso, L., Gómez-Chova, L., Vila-Francés, J., Amorós-López, J., Guanter, L., Calpe, J., Moreno, J., 2008. Improved Fraunhofer line discrimination method for vegetation fluorescence quantification. IEEE Geosci. Remote Sens. Lett. 5 (4), 620–624.

Badgley, G., Field, C.B., Berry, J.A., 2017. Canopy near-infrared reflectance and terrestrial photosynthesis. Sci. Adv. 3 (3), e1602244.

Baker, N.R., 2008. Chlorophyll fluorescence: a probe of photosynthesis in vivo. Annu. Rev. Plant Biol. 59, 89–113.

Baldocchi, D.D., Ryu, Y., Dechant, B., Eichelmann, E., Hemes, K., Ma, S., Verfaillie, J., 2020. Outgoing near infrared radiation from vegetation scales with canopy photosynthesis across a spectrum of function, structure, physiological capacity and weather. J. Geophys. Res. Biogeosci. 125 (7), 1–17 e2019JG005534.

Berk, A., Anderson, G.P., Acharya, P.K., Bernstein, L.S., Muratov, L., Lee, J., Lockwood, R.B., 2005, June. MODTRAN 5: a reformulated atmospheric band model with auxiliary species and practical multiple scattering options: Update. In: Algorithms and Technologies for Multispectral, Hyperspectral, and Ultraspectral Imagery XI, vol. 5806. International Society for Optics and Photonics, pp. 662–667.

Chen, X., Mo, X., Hu, S., Liu, S., 2019. Relationship between fluorescence yield and photochemical yield under water stress and intermediate light conditions. J. Exp. Bot. 70 (1), 301–313.

Cogliati, S., Verhoef, W., Kraft, S., Sabater, N., Alonso, L., Vicent, J., Colombo, R., 2015. Retrieval of sun-induced fluorescence using advanced spectral fitting methods. Remote Sens. Environ. 169, 344–357.

Dechant, B., Ryu, Y., Badgley, G., Zeng, Y., Berry, J.A., Zhang, Y., Li, J., 2020. Canopy structure explains the relationship between photosynthesis and sun-induced chlorophyll fluorescence in crops. Remote Sens. Environ. 241, 111733.

ESA report, 2012. HYFLEX: Technical Assistance for the Deployment of an Advanced Hyperspectral Imaging Sensor during HYFLEX. In: Final Report HYFLEX. https://doi.org/10.5270/esa-nzmrqj3.

ESA report, 2015. Technical Assistance for the Deployment of an advanced hyperspectral imaging sensor during SoyFLEX. In: Final Report. https://doi.org/10.5270/ESA-50a3dd4. SoyFLEX.

Flexas, J., Escalona, J.M., Evain, S., Gulías, J., Moya, I., Osmond, C.B., Medrano, H., 2002. Steady-state chlorophyll fluorescence (Fs) measurements as a tool to follow variations of net CO_2 assimilation and stomatal conductance during water-stress in C3 plants. Physiol. Plant. 114 (2), 231–240.

Flexas, J., Loreto, F., Medrano, H., 2012. Terrestrial Photosynthesis in a Changing Environment: A Molecular, Physiological, and Ecological Approach. Cambridge University Press, Cambridge.

Frankenberg, C., Fisher, J.B., Worden, J., Badgley, G., Saatchi, S.S., Lee, J.E., Yokota, T., 2011. New global observations of the terrestrial carbon cycle from GOSAT: patterns of plant fluorescence with gross primary productivity. Geophys. Res. Lett. 38 (17).

Gamon, J.A., Field, C.B., Goulden, M.L., Griffin, K.L., Hartley, A.E., Joel, G., Valentini, R., 1995. Relationships between NDVI, canopy structure, and photosynthesis in three Californian vegetation types. Ecol. Appl. 5 (1), 28–41.
Gomez-Chova, L., Alonso-Chorda, L., Amoros Lopez, J., Vila Frances, J., del Valle Tascon, S., Calpe, J., Moreno, J., 2006, August. Solar induced fluorescence measurements using a field spectroradiometer. In: AIP Conference Proceedings, vol. 852. American Institute of Physics, pp. 274–281. No. 1.
Guan, K., Berry, J.A., Zhang, Y., Joiner, J., Guanter, L., Badgley, G., Lobell, D.B., 2016. Improving the monitoring of crop productivity using spaceborne solar-induced fluorescence. Glob. Chang. Biol. 22 (2), 716–726.
Guanter, L., Zhang, Y., Jung, M., Joiner, J., Voigt, M., Berry, J.A., Frankenberg, C., Huete, A.R., Zarco-Tejada, P., Lee, J.E., Moran, M.S., 2014. Global and time-resolved monitoring of crop photosynthesis with chlorophyll fluorescence. Proc. Natl. Acad. Sci. 111 (14), E1327–E1333.
Guanter, L., Aben, I., Tol, P., Krijger, J.M., Hollstein, A., Köhler, P., Landgraf, J., 2015. Potential of the TROPOspheric Monitoring Instrument (TROPOMI) onboard the Sentinel-5 Precursor for the monitoring of terrestrial chlorophyll fluorescence. Atmos. Meas. Tech. 8 (3), 1337–1352.
Hao, D., Zeng, Y., Qiu, H., Biriukova, K., Celesti, M., Migliavacca, M., Rossini, M., Asrar, G.R., Chen, M., 2021. Practical approaches for normalizing directional solar-induced fluorescence to a standard viewing geometry. Remote Sen. Environ. 255, 112171.
He, L., Chen, J.M., Liu, J., Mo, G., Joiner, J., 2017. Angular normalization of gome-2 sun-inducedchlorophyll fluorescence observation as a better proxy of vegetation productivity. Geophys. Res. Lett. 440 (11), 0 5691–5699.
He, L., Wood, J.D., Sun, Y., Magney, T., Dutta, D., Köhler, P., Frankenberg, C., 2020. Tracking seasonal and interannual variability in photosynthetic downregulation in response to water stress at a temperate deciduous forest. J. Geophys. Res. Biogeosci. 125 (8) e2018JG005002.
Helm, L.T., Shi, H., Lerdau, M.T., Yang, X., 2020. Solar-induced chlorophyll fluorescence and short-term photosynthetic response to drought. Ecol. Appl. 30 (5), e02101.
Jonard, F., De Cannière, S., Brüggemann, N., Gentine, P., Gianotti, D.J.S., Lobet, G., Vereecken, H., 2020. Value of sun-induced chlorophyll fluorescence for quantifying hydrological states and fluxes: current status and challenges. Agric. For. Meteorol. 291, 108088.
Kaufmann, et al., 2000. Effect of orbital drift and sensor changes on the time series of AVHRR vegetation index data. IEEE Trans. Geosci. Remote Sens. 38, 2584–2597.
Li, X., Xiao, J., He, B., Altaf Arain, M., Beringer, J., Desai, A.R., Noe, S.M., 2018. Solar-induced chlorophyll fluorescence is strongly correlated with terrestrial photosynthesis for a wide variety of biomes: first global analysis based on OCO-2 and flux tower observations. Glob. Chang. Biol. 24 (9), 3990–4008.
Liu, L., Guan, L., Liu, X., 2017. Directly estimating diurnal changes in GPP for C3 and C4 crops using far-red sun-induced chlorophyll fluorescence. Agric. For. Meteorol. 232, 1–9.
Liu, X., Guanter, L., Liu, L., Damm, A., Malenovsky, Z., Rascher, U., Peng, D., Du, S., Gastellu-Etchegorry, J.P., 2019. Downscaling of solar-induced chlorophyll fluorescence from canopy level to photosystem level using a random forest model. Remote Sens. Environ. 231, 110772.
Liu, L., Liu, X., Chen, J., Du, S., Ma, Y., Qian, X., Peng, D., 2020. Estimating maize GPP using near-infrared radiance of vegetation. Sci. Remote Sens. 2, 100009.
Lonbani, M., Arzani, A., 2011. Morpho-physiological traits associated with terminal drought stress tolerance in triticale and wheat. Agron. Res. 9 (1–2), 315–329.
Magney, T.S., Bowling, D.R., Logan, B.A., Grossmann, K., Stutz, J., Blanken, P.D., Lopez, S., 2019. Mechanistic evidence for tracking the seasonality of photosynthesis with solar-induced fluorescence. Proc. Natl. Acad. Sci. 116 (24), 11640–11645.
Magney, T.S., Barnes, M.L., Yang, X., 2020. On the covariation of chlorophyll fluorescence and photosynthesis across scales. Geophys. Res. Lett. e2020GL091098.
Mohammed, G.H., Colombo, R., Middleton, E.M., Rascher, U., van der Tol, C., Nedbal, L., Joiner, J., 2019. Remote sensing of solar-induced chlorophyll fluorescence (SIF) in vegetation: 50 years of progress. Remote Sens. Environ. 231, 111177.
Ollinger, S.V., 2011. Sources of variability in canopy reflectance and the convergent properties of plants. New Phytol. 189 (2), 375–394.
Porcar-Castell, A., Tyystjärvi, E., Atherton, J., van der Tol, C., Flexas, J., Pfündel, E.E., Berry, J.A., 2014. Linking chlorophyll a fluorescence to photosynthesis for remote sensing applications: mechanisms and challenges. J. Exp. Bot. 65 (15), 4065–4095.
Rascher, U., Alonso, L., Burkart, A., Cilia, C., Cogliati, S., Colombo, R., Hyvärinen, T., 2015. Sun-induced fluorescence–a new probe of photosynthesis: first maps from the imaging spectrometer HyPlant. Glob. Chang. Biol. 21 (12), 4673–4684.
Romero, J.M., Cordon, G.B., Lagorio, M.G., 2018. Modeling re-absorption of fluorescence from the leaf to the canopy level. Remote Sens. Environ. 204 (0), 138–146.
Sanchez, R.A., Hall, A.J., Trapani, N., De Hunau, R.C., 1983. Effects of water stress on the chlorophyll content, nitrogen level and photosynthesis of leaves of two maize genotypes. Photosynth. Res. 4 (1), 35–47.
Siegmann, B., Alonso, L., Celesti, M., Cogliati, S., Colombo, R., Damm, A., Kraska, T., 2019. The high-performance airborne imaging spectrometer HyPlant—from raw images to top-of-canopy reflectance and fluorescence products: introduction of an automatized processing chain. Remote Sens. 11 (23), 2760.
Siegmann, B., Cendrero-Mateo, M.P., Cogliati, S., Damm, A., Gamon, J., Herrera, D., Rascher, U., 2021. Downscaling of far-red solar-induced chlorophyll fluorescence of different crops from canopy to leaf level using a diurnal data set acquired by the airborne imaging spectrometer HyPlant. Remote Sens. Environ. 264, 112609.
Simmer, C., Thiele-Eich, I., Masbou, M., Amelung, W., Bogena, H., Crewell, S., Kemna, A., 2015. Monitoring and modeling the terrestrial system from pores to catchments: the transregional collaborative research center on patterns in the soil–vegetation–atmosphere system. Bull. Am. Meteorol. Soc. 96 (10), 1765–1787.
Sun, Y., Fu, R., Dickinson, R., Joiner, J., Frankenberg, C., Gu, L., Fernando, N., 2015. Drought onset mechanisms revealed by satellite solar-induced chlorophyll fluorescence: insights from two contrasting extreme events. J. Geophys. Res. Biogeosci. 120 (11), 2427–2440.
Sun, Y., Frankenberg, C., Wood, J.D., Schimel, D.S., Jung, M., Guanter, L., Gu, L., 2017. OCO-2 advances photosynthesis observation from space via solar-induced chlorophyll fluorescence. Science 358 (6360).
Turner, A.J., Köhler, P., Magney, T.S., Frankenberg, C., Fung, I., Cohen, R.C., 2020. A double peak in the seasonality of California's photosynthesis as observed from space. Biogeosciences 17 (2), 405–422.
van der Tol, C., Verhoef, W., Timmermans, J., Verhoef, A., Su, Zhongbo, 2009. An integrated model of soil-canopy spectral radiances, photosynthesis, fluorescence, temperature and energy balance. Biogeosciences 60 (12), 0 3109–3129.
van der Tol, C., Berry, J.A., Campbell, P.K.E., Rascher, U., 2014. Models of fluorescence and photosynthesis for interpreting measurements of solar-induced chlorophyll fluorescence. J. Geophys. Res. Biogeosci. 119 (12), 2312–2327.
van Wittenberghe, S., Alonso, L., Verrelst, J., Hermans, I., Delegido, J., Veroustraete, F., Samson, R., 2013. Upward and downward solar-induced chlorophyll fluorescence yield indices of four tree species as indicators of traffic pollution in Valencia. Environ. Pollut. 173, 29–37.
Vilfan, N., Van der Tol, C., Muller, O., Rascher, U., Verhoef, W., 2016. Fluspect-B: a model for leaf fluorescence, reflectance and transmittance spectra. Remote Sens. Environ. 186, 596–615.
Wang, C., Guan, K., Peng, B., Chen, M., Jiang, C., Zeng, Y., Frankenberg, C., 2020. Satellite footprint data from OCO-2 and TROPOMI reveal significant spatio-temporal and inter-vegetation type variabilities of solar-induced fluorescence yield in the US Midwest. Remote Sens. Environ. 241, 111728.
Wen, J., Köhler, P., Duveiller, G., Parazoo, N.C., Magney, T.S., Hooker, G., Sun, Y., 2020. A framework for harmonizing multiple satellite instruments to generate a long-term global high spatial-resolution solar-induced chlorophyll fluorescence (SIF). Remote Sens. Environ. 239, 111644.
Werner, C., Correia, O., Beyschlag, W., 1999. Two different strategies of Mediterranean macchia plants to avoid photoinhibitory damage by excessive radiation levels during summer drought. Acta Oecol. 20 (1), 15–23.
Wieneke, S., Ahrends, H., Damm, A., Pinto, F., Stadler, A., Rossini, M., Rascher, U., 2016. Airborne based spectroscopy of red and far-red sun-induced chlorophyll fluorescence: implications for improved estimates of gross primary productivity. Remote Sens. Environ. 184, 654–667.
Wieneke, S., Burkart, A., Cendrero-Mateo, M.P., Julitta, T., Rossini, M., Schickling, A., Rascher, U., 2018. Linking photosynthesis and sun-induced fluorescence at sub-daily to seasonal scales. Remote Sens. Environ. 219, 247–258.
Wohlfahrt, G., Gerdel, K., Migliavacca, M., Rotenberg, E., Tatarinov, F., Müller, J., Yakir, D., 2018. Sun-induced fluorescence and gross primary productivity during a heat wave. Sci. Rep. 8 (1), 1–9.
Wu, G., Guan, K., Jiang, C., Peng, B., Kimm, H., Chen, M., Moore, C.E., 2020. Radiance-based NIRv as a proxy for GPP of corn and soybean. Environ. Res. Lett. 15 (3), 034009.
Xu, S., Atherton, J., Riikonen, A., Zhang, C., Oivukkamäki, J., MacArthur, A., Porcar-Castell, A., 2021. Structural and photosynthetic dynamics mediate the response of SIF to water stress in a potato crop. Remote Sens. Environ. 263, 112555.
Yang, X., Tang, J., Mustard, J.F., Lee, J.E., Rossini, M., Joiner, J., Richardson, A.D., 2015. Solar-induced chlorophyll fluorescence that correlates with canopy photosynthesis on diurnal and seasonal scales in a temperate deciduous forest. Geophys. Res. Lett. 42 (8), 2977–2987.
Yang, P., van der Tol, C., Verhoef, W., Damm, A., Schickling, A., Kraska, T., Rascher, U., 2019. Using reflectance to explain vegetation biochemical and structural effects on sun-induced chlorophyll fluorescence. Remote Sens. Environ. 231, 110996.
Yang, P., van der Tol, C., Campbell, P.K., Middleton, E.M., 2020. Fluorescence Correction Vegetation Index (FCVI): a physically based reflectance index to separate physiological and non-physiological information in far-red sun-induced chlorophyll fluorescence. Remote Sens. Environ. 240, 111676.
Yoshida, Y., Joiner, J., Tucker, C., Berry, J., Lee, J.E., Walker, G., Wang, Y., 2015. The 2010 Russian drought impact on satellite measurements of solar-induced chlorophyll fluorescence: insights from modeling and comparisons with parameters derived from satellite reflectances. Remote Sens. Environ. 166, 163–177.
Zeng, Y., Badgley, G., Dechant, B., Ryu, Y., Chen, M., Berry, J.A., 2019. A practical approach for estimating the escape ratio of near-infrared solar-induced chlorophyll fluorescence. Remote Sens. Environ. 232, 111209.
Zeng, Y., Badgley, G., Chen, M., Li, J., Anderegg, L.D., Kornfeld, A., Berry, J.A., 2020. A radiative transfer model for solar induced fluorescence using spectral invariants theory. Remote Sens. Environ. 240, 111678.
Zhang, Z., Zhang, Y., Joiner, J., Migliavacca, M., 2018. Angle matters: bidirectional effects impact the slope of relationship between gross primary productivity and sun-induced chlorophyll fluorescence from orbiting carbon Observatory-2 across biomes. Glob. Chang. Biol. 24 (11), 5017–5020.
Zhang, Z., Zhang, Y., Porcar-Castell, A., Joiner, J., Guanter, L., Yang, X., Martini, D., 2020. Reduction of structural impacts and distinction of photosynthetic pathways in a global estimation of GPP from space-borne solar-induced chlorophyll fluorescence. Remote Sens. Environ. 240, 111722.